Kim, H., Clauer, C. R., Engebretson, M. J., Matzka, J., Sibeck, D. G., Singer, H. J., Stolle, C., Weimer, D. R., Xu, Z.(2015): Conjugate observations of traveling convection vortices associated with transient events at the magnetopause. - *Journal of Geophysical Research*, *120*, 3, p. 2015-2035.

DOI: http://doi.org/10.1002/2014JA020743

AGU PUBLICATIONS

JGR

Journal of Geophysical Research: Space Physics

RESEARCH ARTICLE

10.1002/2014JA020743

Key Points:
- Space and ground observations of transient events at the magnetopause
- Traveling convection vortices during the transient events in both hemispheres
- Interhemispheric asymmetry found in the TCV structures

Correspondence to:
H. Kim,
hmkim@vt.edu

Citation:
Kim, H., C. R. Clauer, M. J. Engebretson, J. Matzka, D. G. Sibeck, H. J. Singer, C. Stolle, D. R. Weimer, and Z. Xu (2015), Conjugate observations of traveling convection vortices associated with transient events at the magnetopause, *J. Geophys. Res. Space Physics*, *120*, 2015–2035, doi:10.1002/2014JA020743.

Received 16 OCT 2014
Accepted 19 FEB 2015
Accepted article online 25 FEB 2015
Published online 28 MAR 2015

Conjugate observations of traveling convection vortices associated with transient events at the magnetopause

H. Kim[1], C. R. Clauer[1], M. J. Engebretson[2], J. Matzka[3], D. G. Sibeck[4], H. J. Singer[5], C. Stolle[3], D. R. Weimer[1], and Z. Xu[1]

[1]Center for Space Science and Engineering Research and Department of Electrical and Computer Engineering, Virginia Polytechnic Institute and State University, Blacksburg, Virginia, USA, [2]Department of Physics, Augsburg College, Minneapolis, Minnesota, USA, [3]Helmholtz Centre Potsdam, GFZ, German Research Centre for Geosciences, Potsdam, Germany, [4]NASA Goddard Space Flight Center, Greenbelt, Maryland, USA, [5]Space Weather Prediction Center, NOAA, Boulder, Colorado, USA

Abstract Traveling convection vortices (TCVs) are generally produced by field-aligned currents (FACs) at high latitudes associated with transient changes of the magnetopause. This paper presents multipoint conjugate observations of transient events at the magnetopause measured in space and on the ground. The transient events showing radial fluctuation of the magnetopause in association with sudden increases in solar wind dynamic pressure were detected by both the Time History of Events and Macroscale Interactions during Substorms and the Geostationary Operational Environmental Satellite spacecraft. Geomagnetic signatures seen as TCVs in response to the transient events were observed by the ground magnetometer array in Greenland and Canada and their conjugate locations in Antarctica including recently developed Antarctic magnetometers, mostly located along the 40° magnetic meridian. This new conjugate network provides a unique opportunity to observe geomagnetic field signatures over a relatively large region in both hemispheres. This study focuses mainly on the spatial and temporal features of the TCVs in the conjugate hemispheres in relation to the transient events at the magnetopause. The TCV events are characterized by their single or twin vortex, of which the centers are located approximately at 72°–76° magnetic latitude, propagating either dawnward or duskward away from local noon. While interhemispheric conjugacy is expected with an assumption that TCV signatures are created by FACs directed in both hemispheres, our observations suggest that there might be more complex mechanisms contributing the asymmetrical features, perhaps due to field line mapping and/or conductivity differences.

1. Introduction

Transient events with durations of approximately a few minutes to half an hour are common in dayside magnetometer data and observed as a rapid increase of the geomagnetic fields at low latitudes and midlatitudes (sudden impulse or SI) and magnetic impulse events (MIE) at high latitudes [e.g., *Araki*, 1977; *Russell et al.*, 1994; *Lanzerotti et al.*, 1991; *Sibeck*, 1993; *Sitar et al.*, 1996]. A particular type of MIE is traveling convection vortices (TCVs) characterized by the vortical structure of ionospheric convection propagating longitudinally from the dayside to tailside. High-latitude ground observations by *Friis-Christensen et al.* [1988] and *Glassmeier et al.* [1989] are the first two important studies of TCVs.

In a magnetogram from a single high-latitude ground station, TCVs are typically seen as a bipolar deflection (positive to negative or vice versa) mainly in the horizontal (H) component with frequencies approximately in the Pc5 range (2–7 mHz). Using longitudinally spaced stations, the "traveling" and "vortical" structures can be observed. The ionospheric pattern during TCVs is accounted for the effect of circular Hall currents (see *Fukushima* [1969] for "Fukushima's Theorem") produced by a pair of oppositely directed moving field-aligned current (FAC) system [*McHenry and Clauer*, 1987; *Friis-Christensen et al.*, 1988; *Glassmeier et al.*, 1989; *Kivelson and Southwood*, 1991; *Sibeck et al.*, 2003]. A FAC flows upward from the center of a clockwise vortex and downward into the center of a counterclockwise vortex in the Northern Hemisphere and vice versa in the Southern Hemisphere [*Cowley*, 2000]. TCVs propagate with velocities of ~3–10 km/s in the ionosphere, and their ionospheric-scale size ranges approximately between 1000 and 3000 km occurring as transient deflections of several hundreds of nanotesla with maximum occurrences at ~73–75° magnetic latitudes [*Friis-Christensen et al.*, 1988; *Glassmeier et al.*, 1989; *Glassmeier and Heppner*, 1992; *Zesta et al.*, 1999; *Amm et al.*, 2002; *Murr et al.*, 2002; *Zesta et al.*, 2002; *Fillingim et al.*, 2011].

Generation mechanisms of transient TCVs have been attributed to interaction processes between the solar wind and the magnetosphere such as bursty merging (or flux transfer events (FTE)) [*Goertz et al.*, 1985; *Lanzerotti et al.*, 1987] and solar wind dynamic pressure pulse interactions with the magnetopause [*Friis-Christensen et al.*, 1988; *Glassmeier and Heppner*, 1992; *Sibeck et al.*, 1989, 2003]. The bursty merging appears to occur on the dayside equatorial magnetopause preferentially for southward interplanetary magnetic field (IMF) orientations and is typically not associated with transient changes in the solar wind parameters. Kelvin-Helmholtz instabilities (KHI) have been attributed to the generation of periods of continuous TCVs propagating antisunward lasting for an hour or more [*McHenry et al.*, 1990; *Clauer and Ridley*, 1995; *Clauer and Petrov*, 2002; *Clauer*, 2003; *Dougal et al.*, 2013]. Since we are concerned here with transient impulsive events, we do not consider FTE and KHI further in this analysis.

Although multiple mechanisms are likely to generate TCVs, a number of observations [e.g., *Sitar et al.*, 1998; *Zesta et al.*, 1999; *Murr and Hughes*, 2003; *Kataoka et al.*, 2003; *Sibeck et al.*, 2003] and numerical simulations [e.g., *Kivelson and Southwood*, 1991; *Kataoka et al.*, 2004] support the idea that solar wind impulsive dynamic pressure events are a major source for impulsive TCVs. Transient compression of the magnetosphere due to pressure changes at the magnetopause or the inner edge of the low-latitude boundary layer (LLBL) produce field-aligned currents (FAC) into and out of the high-latitude ionosphere. Azimuthal pressure gradients associated with the magnetopause compression generate a pair of oppositely directed FAC and thus a pair of oppositely rotating vortical structures in the ionosphere.

Transient events associated with compression of the magnetopause due to pressure changes have also been reported using spacecraft at or near the boundary [e.g., *Korotova et al.*, 2011; *Turner et al.*, 2011; *Zhang et al.*, 2012] and at geosynchronous orbit [e.g., *Lee and Lyons*, 2004; *Villante and Piersanti*, 2011]. Where FACs associated with TCVs map in the magnetosphere is still, however, a challenging question. In an effort to answer this question, studies have used auroral imagers or low-altitude satellites to observe particle precipitation associated with TCVs, locating the source near the boundary plasma sheet-LLBL interface [*Sitar et al.*, 1998], within the central plasma sheet [*Murr et al.*, 2002], and near the open-closed field line boundary [*Moretto and Yahnin*, 1998; *Engebretson et al.*, 2013].

Observational studies have shown that TCVs are conjugate phenomena [e.g., *Kataoka et al.*, 2001; *Murr et al.*, 2002]. Simultaneous observations of TCVs in both hemispheres are, however, considered challenging mainly due to the fewer number of ground instruments in the Southern Hemisphere. While it is often assumed that the two hemispheres behave with good conjugacy (mainly for simplicity in modeling or observations), studies have indicated that interhemispheric asymmetry in response to solar wind discontinuities might be more significant than often thought. *Kim et al.* [2013] investigate conjugate behavior of MIEs in response to solar wind pressure impulse events, showing interhemispheric behavior that is not quite conjugate. From multi-instrument observations of a TCV event associated with the FAC system, *Murr et al.* [2002] suggested that the overall nature of the TCV event at the conjugate points is similar, including an upward and then downward FAC pair, the amplitude of the perturbations, the propagation speed, and the spatial scale. However, from the magnetometer and riometer signatures, they found a time delay between the two hemispheres with the event in the Southern Hemisphere being delayed by 2 min, while the perturbations were similar in shape and amplitude.

This paper presents observations of transient events near the magnetopause associated with sudden increases in solar wind dynamic pressure and their ground responses seen as TCVs. The results reported here are unique because we also include observations of the transient events near the magnetopause, inner magnetospheric signatures measured at geostationary orbit, and conjugate ground-based measurements. The confluence of satellites and ground observations to permit such a thorough examination of events is very rare. The transient events were detected by both the Time History of Events and Macroscale Interactions during Substorms (THEMIS) and Geostationary Operational Environmental Satellite (GOES) spacecraft and the ground signatures by ground-based magnetometer arrays in the Northern and Southern Hemispheres. Newly developed low-power magnetometers have been recently deployed in the Antarctic plateau, establishing measurement points conjugate to the existing Greenland west coast magnetometer array along the 40° magnetic meridian. This new conjugate network provides a unique opportunity to observe simultaneous geomagnetic field signatures over a relatively large region in both hemispheres. Well-defined TCVs observed during the initial operation of the new ground network are presented in

this paper to examine conjugate behavior of ionospheric convection in response to transient events in the magnetosphere.

2. Data Set

High-resolution (1 min) OMNI (spacecraft-interspersed, near-Earth solar wind data) IMF and plasma data time-shifted to the nose of the Earth's bow shock [*King and Papitashvili*, 2005] are used to examine solar wind plasma parameters. THEMIS Data Analysis Software (TDAS) is used to plot the OMNI data which are based on the OMNI database (http://omniweb.gsfc.nasa.gov) processed from magnetic field and plasma measurements recorded by the Advanced Composition Explorer (ACE), Wind, Interplanetary Monitoring Platform-8 (IMP-8), and Geotail spacecraft. Magnetic field data (~3 s resolution) from the THEMIS-A, THEMIS-D, and THEMIS-E spacecraft [*Auster et al.*, 2008] are used to show magnetic field perturbations near the magnetopause and also accessed through TDAS. Magnetic field data (~4 s resolution) from the Cluster spacecraft [*Balogh et al.*, 1997] are obtained using the NASA CDAWeb at http://cdaweb.gsfc.nasa.gov. GOES magnetometer data (13 and 15, 1 min resolution) are also used and accessed using the data archive at National Oceanic and Atmospheric Administration (NOAA) Space Weather Prediction Center (http://www.swpc.noaa.gov).

Ground magnetic field data are obtained by fluxgate magnetometers located in Greenland, Canada, and Antarctica. The Greenland stations are operated by Technical University of Denmark and provide 10 s (time stamped for the beginning of the 10 s interval) magnetic field data. In this paper, data from 14 Greenland stations are presented, most of them located along the 40° magnetic meridian. Data (1 s resolution) from a Canadian station in Iqaluit (IQA), which is operated by Natural Resources Canada (NRCan), are also included to examine longitudinal propagation of the magnetic field perturbations shown in this study. The Antarctic stations include South Pole Station (SPA), three (P01, P03, and P05) of Automated Geophysical Observatories (AGOs) [*Rosenberg and Doolittle*, 1994], and three (PG1, PG2, and PG3) of newly deployed stations called Autonomous Adaptive Low-Power Instrument Platform (AAL-PIP) [*Musko et al.*, 2009; *Clauer et al.*, 2014]. The AAL-PIP systems are deliberately located at magnetically conjugate points paired with the Greenland west coast network. The ground stations used in this study are shown in Table 1 and Figure 1. All of the Antarctic stations provide magnetic field data of 1 s resolution.

All the satellite data in this paper are presented in the Geocentric Solar Ecliptic (GSE) coordinate system except for GOES satellite data. The GOES satellite magnetometers conform to the magnetic northward-earthward-eastward (PEN) coordinate system, in which P is a magnetic field vector component pointing northward, perpendicular to the orbit plane (parallel to Earth's spin axis) and E points earthward, being perpendicular to P. N completes the Cartesian coordinates and points eastward. The geomagnetic coordinates of the ground stations are obtained from the International Geomagnetic Reference Field (IGRF) Corrected Geomagnetic (CGM) model for Epoch 2013. The ground magnetometers conform to the magnetic horizontal-eastward-downward (HEZ) coordinate system, in which H is along the local horizontal magnetic field, Z downward toward the earth, and E completes the right-hand rule pointing eastward in the horizontal plane.

3. Observations

This section presents three transient events observed in space and their ionospheric responses identified as TCVs measured by the ground network on 18 and 19 January 2013. The three transient events are associated with sudden increases in solar wind dynamic pressure ($P_d = n_p \times v_{sw}^2$, where n_p is proton mass density and v_{sw} is solar wind velocity) and constantly northward IMF orientation identified from both ACE and OMNI data. During the events, the three THEMIS spacecraft were fortuitously located near the magnetopause making it possible to detect the transient events while the two GOES spacecraft observed magnetospheric compression. In response to the three transient events, ground data display TCV signatures in both hemispheres, each ground event occurring in the prenoon, noon, and postnoon sectors, respectively. We present here a thorough analysis of the events. For the reader not interested in this complete detail, a summary of the critical parameters either observed or derived for the events is given in Table 2.

3.1. Event 1

Figure 2 shows a transient event observed from (a) OMNI data, (b) THEMIS magnetometer data, (c) GOES magnetometer data, and (d) the satellite orbits during this event on 18 January 2013. The OMNI data

Table 1. Geographic and Geomagnetic Locations of the Magnetometer Stations Presented in This Study[a]

			Geographic		Geomagnetic		
Region	Station	Station Code	Lat. (°)	Long. (°E)	Lat. (°)	Long. (°E)	MLT MN in UT
Northern Hemisphere	Thule	THL	77.47	290.77	84.40	27.48	3.4
	Savissivik	SVS	76.02	294.90	82.68	31.23	3.1
	Kullorsuaq	KUV	74.57	302.82	80.36	40.28	2.4
	Upernavik	UPN	72.78	303.85	78.57	38.71	2.6
	Uunmannaq	UMQ	70.68	307.87	75.99	41.22	2.4
	Qeqertarsuaq	GDH	69.25	306.47	74.82	38.15	2.6
	Attu	ATU	67.93	306.43	73.54	37.09	2.7
	Kangerlussuaq	STF	67.02	309.28	72.14	39.96	2.5
	Iqaluit	IQA	63.75	291.50	71.69	15.16	4.2
	Ittoqqortoormiit	SCO	70.48	338.03	71.24	70.54	0.0
	Maniitsoq	SKT	65.42	307.10	70.93	36.43	2.7
	Nuuk	GHB	64.17	308.27	69.49	37.12	2.7
	Tasiilaq	AMK	65.60	322.37	68.51	52.65	1.5
	Paamiut	FHB	62.00	310.32	66.92	38.43	2.6
	Narsarquaq	NAQ	61.16	314.56	65.23	42.61	2.3
Southern Hemisphere	AGO P03	P03	−82.80	28.60	−72.09	41.03	2.0
	AAL-PIP PG3	PG3	−84.81	37.63	−73.60	36.75	2.4
	South Pole	SPA	−90.00	–	−74.21	19.39	3.6
	AAL-PIP PG2	PG2	−84.42	57.96	−75.33	39.20	2.2
	AAL-PIP PG1	PG1	−84.50	77.20	−77.06	37.55	2.3
	AGO P01	P01	−83.86	129.61	−80.34	17.33	3.8
	AGO P05	P05	−77.24	123.52	−86.96	29.47	2.9

[a]The geomagnetic coordinates of the stations are obtained from the International Geomagnetic Reference Field (IGRF) Corrected Geomagnetic (CGM) model for Epoch 2013.

(Figure 2a) show an increase in solar wind pressure (+14 nPa over 15 min) starting at around 12:35 UT as seen in the fourth panel (grey box 1-1). The increase in the *SYM-H* index (40 nT over 15 min) indicates magnetospheric compression associated with the pressure increase (the fifth panel of Figure 2a). The IMF data (the first panel of Figure 2a) show that the IMF orientation was northward with no remarkable discontinuity during the event. There is another pressure increase (5 nPa) followed by a decrease (4 nPa) associated with a northward IMF between 13:12 and 13:18 UT (grey box 1-2). Note that $Kp = 3$ during Event 1.

Magnetic field variations observed by THEMIS-A, THEMIS-D, and THEMIS-E are shown in the first to fifth panels in Figure 2b, respectively. Inward magnetopause motion is seen by THEMIS-A at around 12:35 UT (~11 MLT), followed by inward bow shock motion at around 12:49 UT. This indicates that the THEMIS spacecraft exited the magnetosphere and entered the magnetosheath characterized by its "noisy" magnetic fields at around 12:38 UT and then entered the solar wind at around 12:49 UT. The other spacecraft, THEMIS-D and THEMIS-E, also observed very similar signatures at slightly different times. The radial magnetospheric motion appears to be associated with the pressure increase shown in the OMNI data (grey box 1-1). Following this event, THEMIS-A observed brief outward and inward motion of the bow shock at around 13:13 UT and 13:17 UT, respectively, which appears to be associated with the second pressure event starting at 13:12 UT as shown in the OMNI data (grey box 1-2). This event is not clearly seen from the THEMIS-D and THEMIS-E data as the two spacecraft were still in the solar wind during the period as can be inferred from the satellite orbit in the GSE X-Y plane shown in Figure 2d. The bow shock location in Figure 2d is obtained using the static model by *Fairfield* [1971]. The magnetopause location in the same figure is estimated using the model by *Shue et al.* [1997], which is a dynamic model that depends on IMF and solar wind dynamic pressure. For Event 1, v_{sw} of 418 km/s, n_p of 4.0 cm^{-3}, and B_z of 13 nT are used as the input parameters for

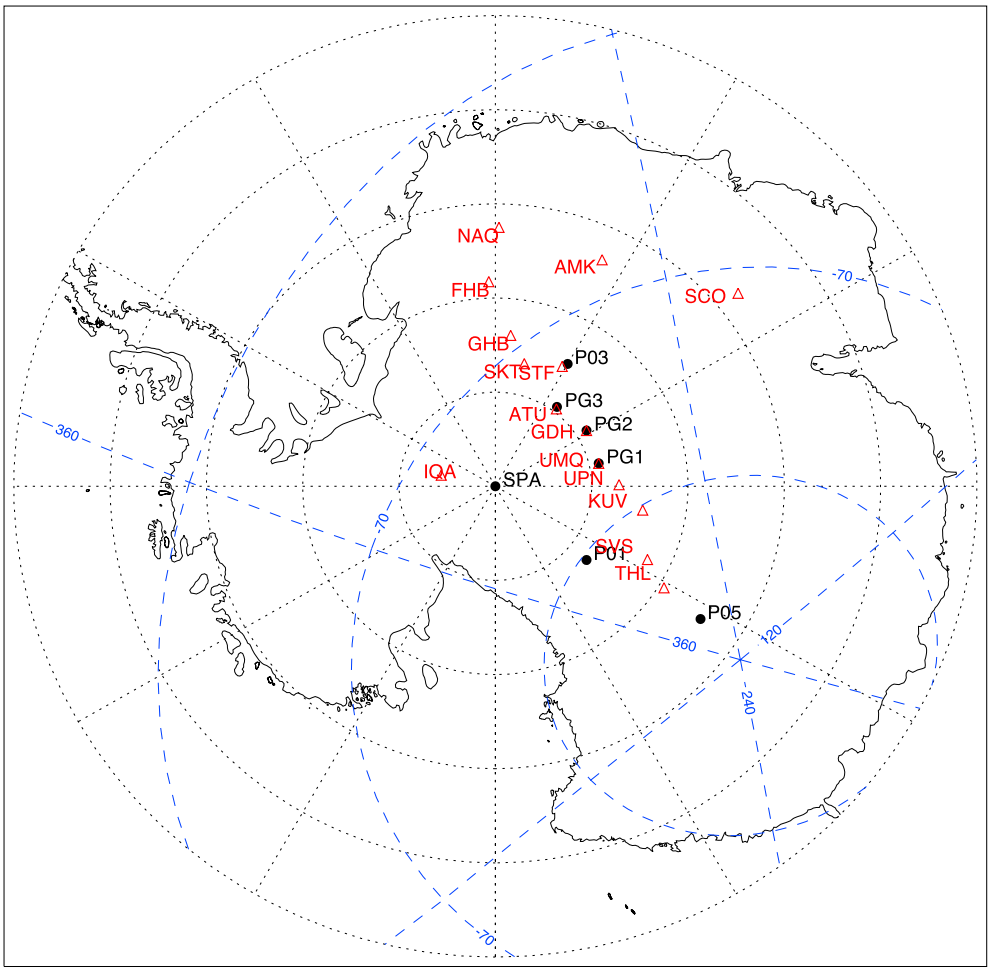

Figure 1. Map of Antarctica showing the locations of the Antarctic stations including South Pole Station (SPA), three (P01, P03, and P05) of the automatic geophysical observatories (AGO), and newly deployed Autonomous Adaptive Low-Power Instrument Platform (AAL-PIP) systems (PG1, PG2, and PG3), marked by the solid black dots. The red triangles indicate the locations of the Greenland and Canadian magnetometer stations mapped to the Antarctic.

the magnetopause model. The symbols in Figure 2d indicate the initial locations of each satellite during the time period shown on top of the panel.

Magnetic field data from GOES-13 and 15 shown in Figure 2c indicate the compression of the magnetosphere associated with the solar wind pressure increases, starting at 12:35 UT. The second event (~13:15 UT) is, however, not clearly registered by the GOES spacecraft. GOES-13, which was located in the morning sector, observed the more pronounced compression than GOES-15 which was located in the predawn sector. The baseline of each component is subtracted from the original GOES satellite data to show magnetic field variations only.

The Cluster satellites (C1 to C4) were also situated near the magnetopause during the event as shown in Figure 2d. Magnetic field data from Cluster show that inward motion was observed at around 12:37 UT (Figure 3). C1, C3, and C4 were in the south lobe before this event, while C2 was closer to the magnetopause and thus measured a more bipolar magnetic field signature. All the Cluster spacecraft exited the magnetosheath at around 12:50 UT when they entered the noisy solar wind and foreshock. The spacecraft then observed brief outward motion of the magnetosheath approximately from 13:22 to 13:24 UT.

Geomagnetic field responses to the solar wind pressure event shown above are clearly detected by the ground network in both hemispheres. Figures 4a and 4b present stacked plots of ground magnetometer data from the Greenland network (one exception is IQA, Canada) and their conjugate stations in Antarctica, respectively, along the 40° magnetic meridian. The CGM coordinates of each station are labeled below each

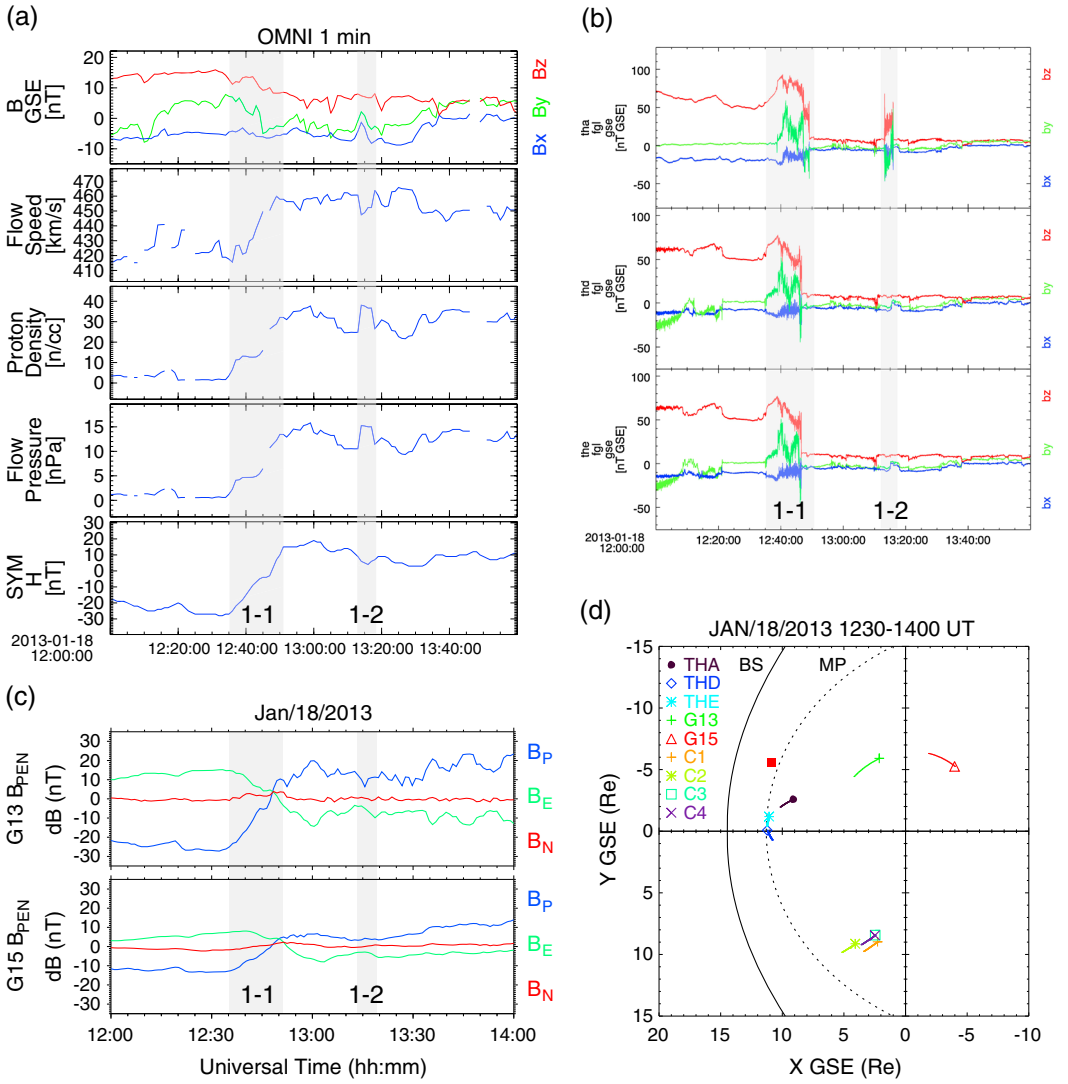

Figure 2. (a) OMNI data; (b) THEMIS magnetic field data; (c) GOES magnetic field data, and (d) satellite orbits during Event 1. The symbols in Figure 2d indicate the initial locations of each satellite during the time period shown on top of the panel. The equatorial intersection of the magnetic field of the ground response is marked with the red rectangle in Figure 2d.

station code. The stations are stacked in order of magnetic latitude, the top plot being the highest (northern stations) and the lowest (southern stations). There are some longitudinally located stations: the IQA-STF and SKT-SCO pairs. The baseline of each component is subtracted from the original ground magnetic field data to show magnetic field variations only and to isolate TCV signatures from the background.

Magnetic field disturbances are observed at around 12:36 UT (10:36 MLT at 40° magnetic longitude), corresponding to the first pressure event observed in space (grey boxes 1-1 in Figure 2). The disturbances seen at around 13:15 UT appear to be associated with the second pressure event (grey box 1-2 in Figure 2). The maximum disturbance is observed from ATU located at 73.5° magnetic latitude (MLAT) in the Northern Hemisphere, while in the Southern Hemisphere, it seems that P03 at −72.1° MLAT measured the maximum disturbance, although it is difficult to assess due to the missing data gap. Moreover, the responses to the second pressure event at 13:15 UT are not as well defined as those in the Northern Hemisphere. The equatorial intersection of the magnetic field of the ground response is marked with the red rectangle in Figure 2d. The intersection points on the magnetospheric equatorial plane are estimated by tracing the magnetic field lines of each ground signature at given positions and times to the equatorial plane using a magnetic field tracing tool (Interactive Data Language (IDL) GEOPACK) based on the IGRF and Tsyganenko model (T01) [*Tsyganenko*, 2002a, 2002b].

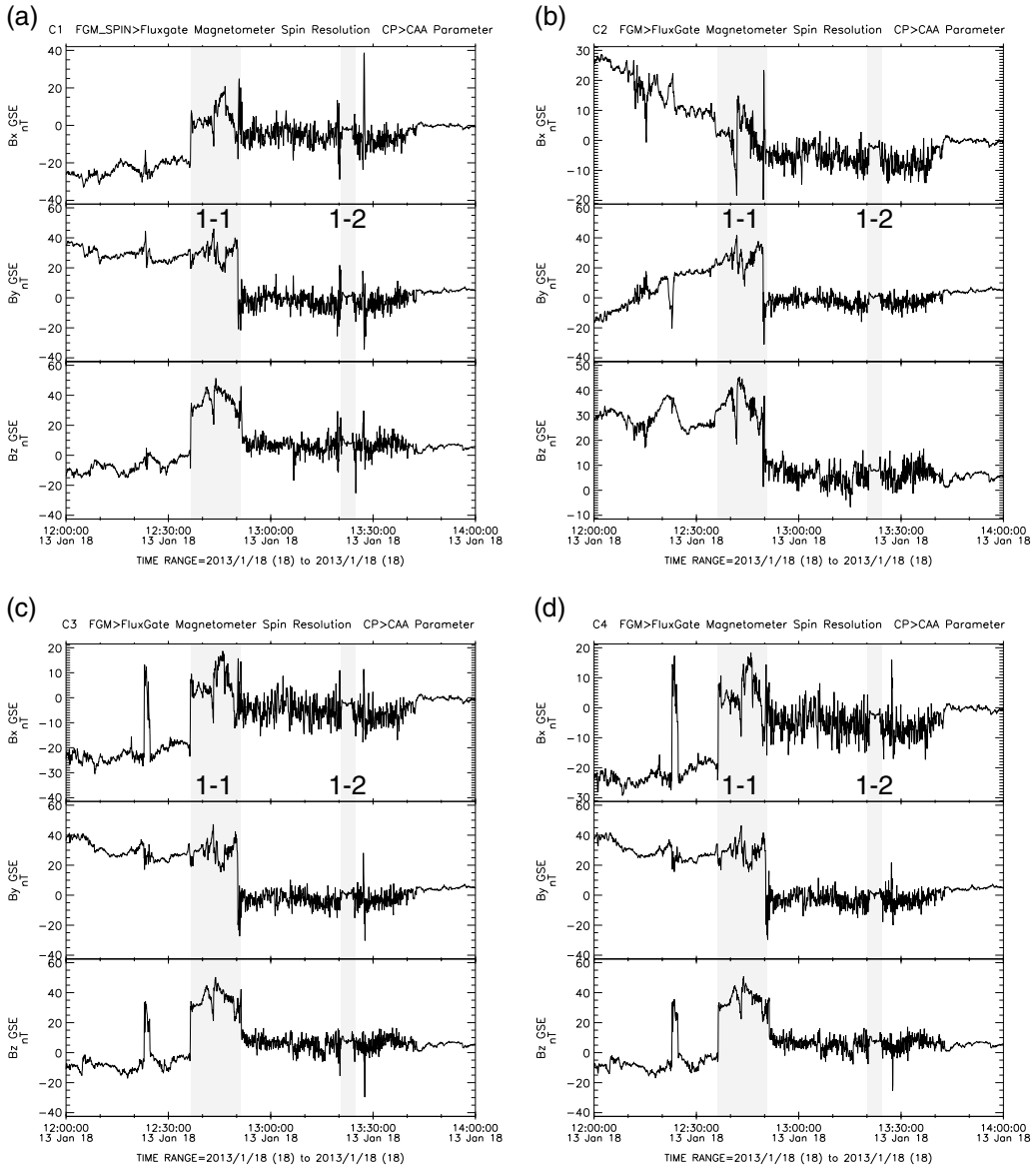

Figure 3. (a to d) Magnetic field data from the Cluster spacecraft, C1 to C4, respectively, during Event 1. The plots are generated using the tool in Coordinated Data Analysis Web (CDAWeb) at http://cdaweb.gsfc.nasa.gov.

Figure 5 shows ionospheric convection flow patterns inferred from the ground magnetometer data during the first pressure event in Event 1. The patterns are displayed by rotating the total horizontal magnetic field vectors averaged over a certain interval (20 s in this study) by 90° clockwise after the baseline of the data are removed to represent $\mathbf{E} \times \mathbf{B}$ convection. The convection patterns obtained from each latitudinal station are stacked in order of latitude, and thus their temporal changes over the latitudinal extent are displayed. The baseline removal is to isolate events of interest from the background. In addition to this process, the latitudinal spaces are filled with interpolated vectors, and thus the patterns are more clearly seen. This is based on an assumption that ionospheric conductivity is uniform over the area of observations. At least for the events shown in this paper, this assumption is reasonable as the events occurred in January when Greenland is under dark conditions while Antarctica is under sunlit conditions. This technique has been widely used in a number of studies [e.g., *Friis-Christensen et al.*, 1988; *Glassmeier et al.*, 1989; *Sitar et al.*, 1998; *Engebretson et al.*, 2013].

A single TCV is clearly seen near 12:41 UT in both hemispheres as shown in Figure 5. While the center of the TCV is observed at ~74° MLAT in the Northern Hemisphere, it is observed at ~76° MLAT in the Southern

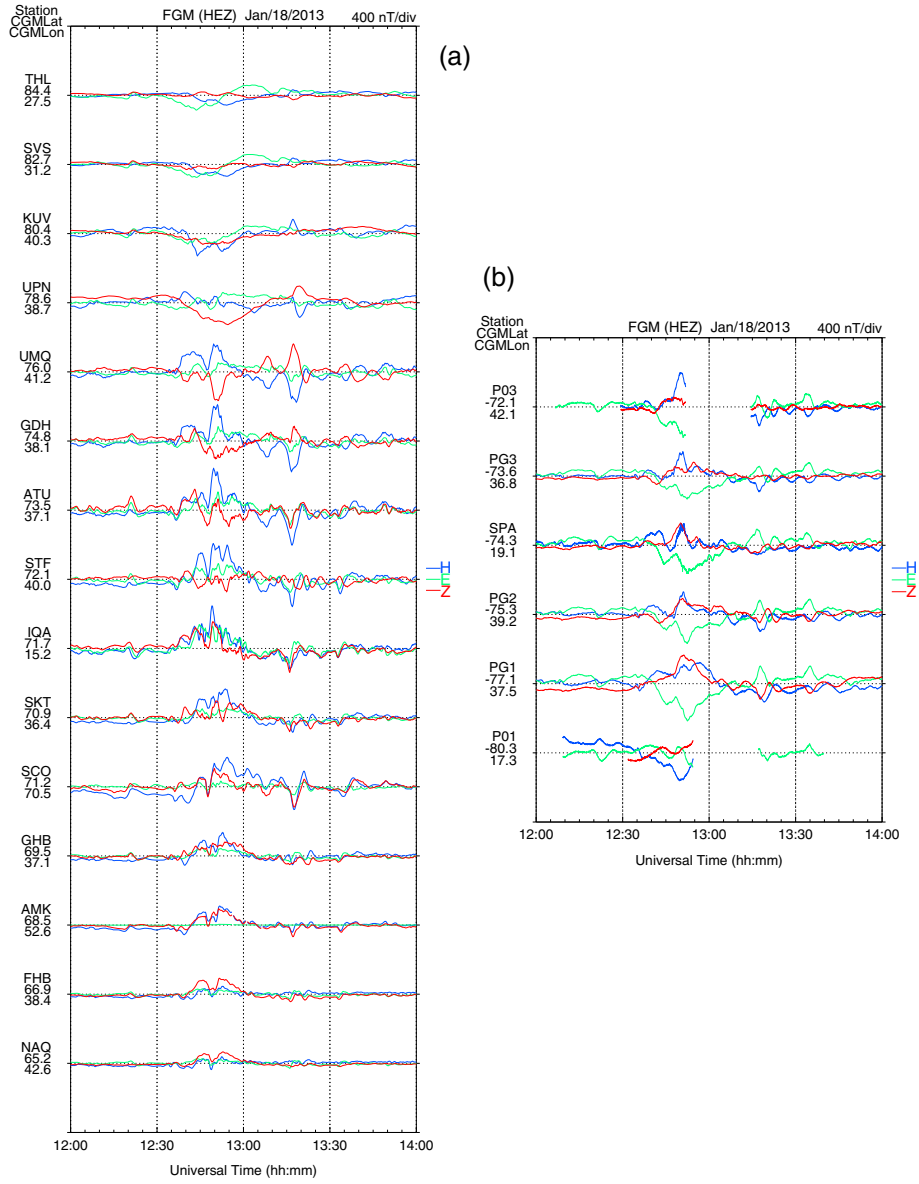

Figure 4. Magnetic field data from (a) ground stations in the Northern Hemisphere and (b) their conjugate stations in the Southern Hemisphere during Event 1.

Hemisphere. There is also a time difference in the TCV occurrences between the Northern and Southern Hemispheres. The center of the TCV appeared at ~12:42:30 UT in the Northern Hemisphere and at ~12:43:20 UT in the Southern Hemisphere. The shapes of the vortex are also different: the vortex in the Southern Hemisphere is more skewed. The second solar wind pressure event starting at ~13:15 UT produced no remarkable ionospheric signatures (figure not shown).

Based on the magnetic field variations observed by THEMIS-D and THEMIS-E during Event 1 (Figure 2b), both of which were located near the boundary of the magnetopause at a similar radial distance of ~11 R_E, the azimuthal propagation velocity of the transient event can be estimated. At the onset of Event 1 (12:35 UT), THEMIS-D was at (11.21, −0.03, 2.64) R_E and THEMIS-E at (11.09, −1.15, 3.16) R_E in the GSE coordinate system. The azimuthal separation between the two spacecraft was 5.8°, which corresponds to ~7100 km at the approximate radial location of the two spacecraft (11 R_E, $L = 11.5$, and invariant latitude (ILAT) = 72.8°). The transient event at THEMIS-E led that at THEMIS-D by 10 s, indicating that the propagation is eastward (duskward) at a speed of 710 km/s near the magnetopause. Using the THEMIS observations and assuming that the angular velocity does not change during the propagation from the magnetopause to the

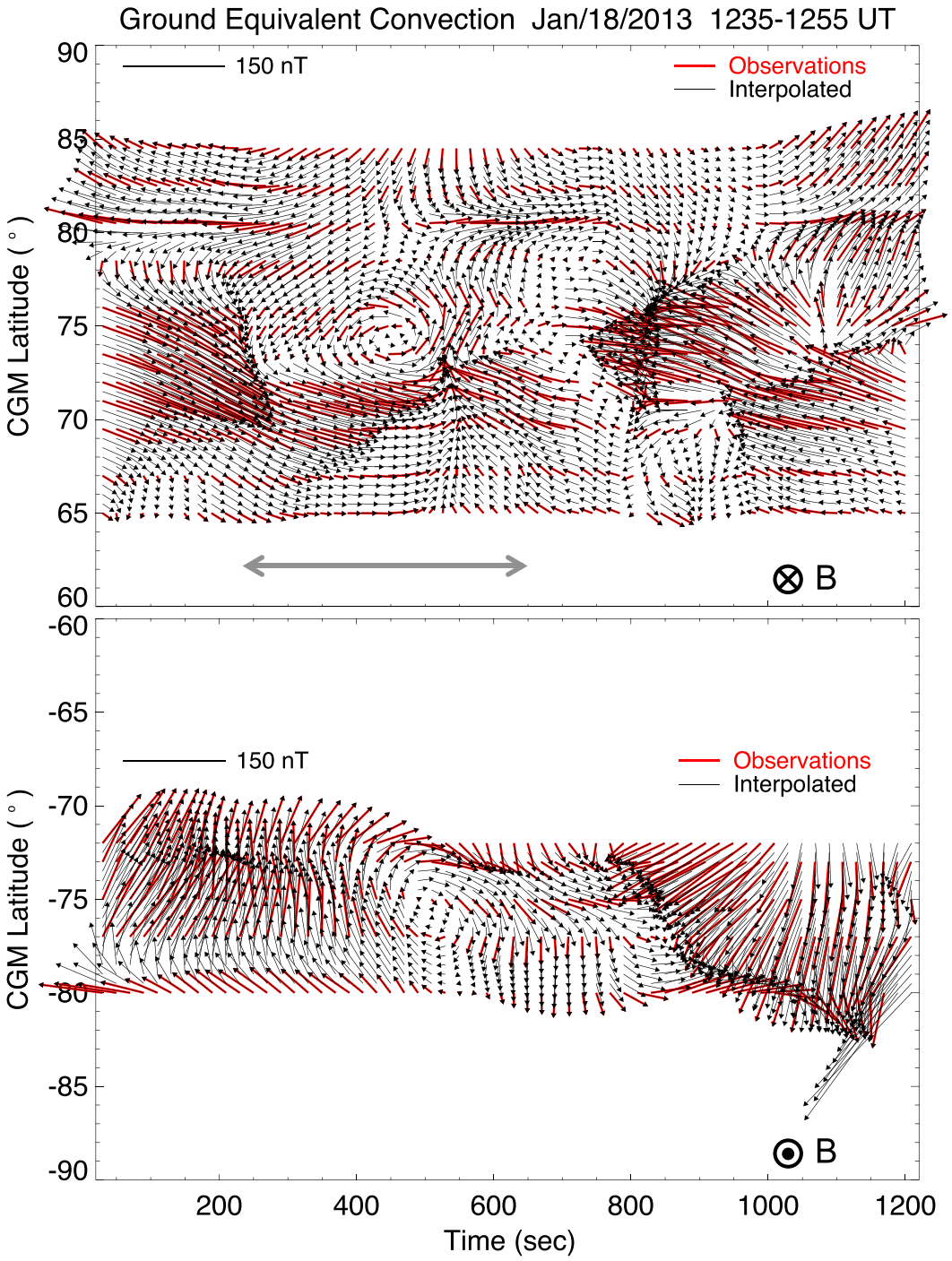

Figure 5. Ground equivalent convection inferred from the magnetic field data during the first pressure event that occurred from 12:35 to 12:55 UT for Event 1. Latitudinally interpolated convection vectors are displayed in black lines overplotted with the observed convection patterns in red lines.

ionosphere, the equivalent ionospheric propagation velocity near the TCV center is 17 km/s on the ground because the longitudinal separation at the ground points is ~170 km and the time lag is 10 s. The propagation speed is quite high and is discussed in section 4.

The azimuthal propagation of the event is also shown in the longitudinally spaced stations, the IQA-STF and SKT-SCO pairs in the Northern Hemisphere and the SPA-PG3 pair in the Southern Hemisphere. The propagation is consistently eastward (IQA to STF, SKT to SCO, and SPA to PG3), in agreement with the

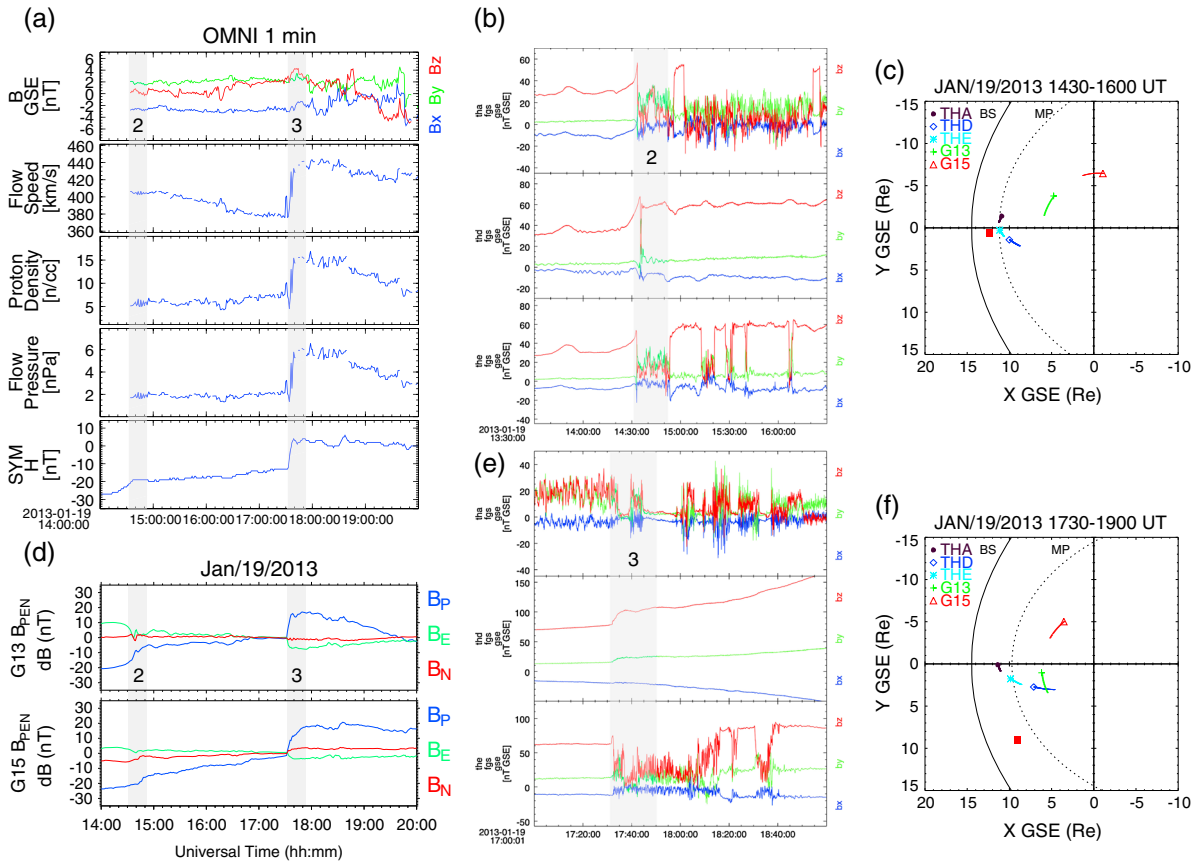

Figure 6. (a) OMNI data; (b and e) THEMIS magnetic field data and (d) GOES magnetic field data during Events 2 (grey box 2) and 3 (grey box 3). (c and f) Satellite orbits during Events 2 and 3, respectively. The symbols in the orbit plots indicate the initial locations of each satellite during the time period shown on top of the panel. The equatorial intersections of the magnetic fields of the ground responses are marked with the red rectangles in Figures 6c and 6f.

THEMIS observations. However, the propagation speed between the two station pairs in the Northern Hemisphere is significantly different. The time lag between the magnetic disturbances at IQA and STF is 67 s, yielding 13.7 km/s (distance between the two stations, 918 km divided by 67 s). The distance and time lag between SKT and SCO are 1388 km and 60 s, yielding 23 km/s. The average propagation velocity in the Northern Hemisphere is thus 18.4 $\pm$ 4.7 km/s. The magnetic signatures in the Southern Hemisphere (SPA-PG3) during this event are rather distorted, making it challenging to estimate the time lag (cross correlation of 0.54): the distance and time lag between the two Antarctic stations are 577 km and 36 s, yielding 16 km/s. Even with the difficulty in the estimation, the propagation speed between the conjugate hemispheres (IQA-STF and SPA-PG3) appears to be in good agreement. Again, IQA and SPA are conjugate stations and so are STF and PG3 (see Table 1). The large propagation speed (23 km/s) observed by the eastward stations, SKT-SCO, is questionable. *Zesta et al.* [2002] excluded TCV events with propagation velocities of >20 km/s in their statistical study because such large propagation velocities projected at the magnetopause are much larger than any possible magnetosheath velocity.

The longitudinal extent of the vortices is estimated using the propagation speed and duration of the event. The grey arrow in Figure 5 indicates the approximate duration of the TCV event in the Northern Hemisphere, which is ~420. Using the average propagation speed of 18.4 km/s, the longitudinal size of the vortex is estimated to be ~7700 km. Although the vortical structure in the Southern Hemisphere is also clearly seen, it is rather difficult to measure the duration because the leading portion of the event appears to be quite distorted and there are no low-latitude measurements. It should be noted that the duration of the event is estimated from visual inspection of the convection patterns and thus the value is very approximate.

3.2. Event 2

Figure 6 shows two transient events observed on 19 January 2013. Two grey boxes denote the periods for Event 2 and Event 3, respectively. Event 2 is discussed in this section and Event 3 in the following section.

While the OMNI data in Figure 6a contain a data gap, we infer a pressure increase to produce the event at 14:30 UT (grey box 2). This impulsive dynamic pressure increase is confirmed in the upstream ACE data (not shown here) where we observe an increase in solar wind flow pressure of 1.5 nPa over about 5 min (note that OMNI data use ACE data as mentioned in section 2). In addition, the *SYM-H* index (fifth panel in Figure 6a) can be interpreted as a magnetospheric compression due to an increase of solar wind pressure producing a field increase of 8 nT over 20 min. The ACE data also show that the IMF orientation was northward with discontinuity predominantly in the IMF B_x component (−5 nT to −2 nT during the impulse event). Note that $Kp = 1$ during this event.

Magnetic field variations observed by THEMIS-A, THEMIS-D, and THEMIS-E are shown in the first to third panels in Figure 6b, respectively. All the spacecraft, which were located near the magnetopause during this event, measured inward motion of the magnetopause. THEMIS-D only briefly moved into the magnetosheath at the peak of the compression (∼20 nT increase in B_z), while THEMIS-A and THEMIS-E observed fluctuating motion of the magnetopause, moving back and forth between the magnetosphere and magnetosheath. For example, THEMIS-A entered the magnetosheath right after the compression at 14:30 UT (∼11:30 MLT), in which the noisy magnetic fields are seen, and returned to the magnetosphere at 14:52 UT for about 5 min in the region. THEMIS-E, which was located near the magnetopause at the Sun-Earth line (see Figure 6c), measured more fluctuating signatures during this event.

Figure 6d shows magnetic field data from GOES-13 and 15, indicating the compression of the magnetosphere associated with the solar wind pressure impulse event at 14:30 UT (grey box 2). The event is more pronounced in the GOES-13 data than the GOES-15 data mainly because GOES-13 was located in the prenoon sector, while GOES-15 was near the dawn sector. The location of the GOES spacecraft during Event 2 is also presented in Figure 6c. For the magnetopause location during this event, v_{sw} of 410 km/s, n_p of 4.0 cm^{-3}, and B_z of 0 nT are used as the input parameters for the magnetopause model.

Geomagnetic field signatures in response to the solar wind pressure event begin at around 14:33 UT (12:33 MLT at 40° magnetic longitude) as shown in Figure 7. A bipolar structure is clearly seen in the ground data in both hemispheres. It appears that the maximum disturbance is observed near the region between ATU at 73.5° MLAT and STF at 72.1° MLAT (among the 40° meridional stations) in the Northern Hemisphere and near SPA at −74.3° MLAT in the Southern Hemisphere. Same as done in the previous example event, the equatorial intersection of the magnetic field of the ground response is marked with the red rectangle in Figure 6c.

Ionospheric convection flow patterns in association with the solar wind pressure impulse at 14:30 UT are presented in Figure 8. A twin vortex is clearly seen in the Northern Hemisphere, while only one vortex is observed in the Southern Hemisphere. The lack of a second vortex in the Southern Hemisphere could be due to the fact that there was no measurement in the region above −72° MLAT if the TCV is skewed equatorward. This needs to be carefully assessed later with more measurement points. The center of the TCVs appeared at ∼73.5° MLAT starting at 14:37 UT in the Northern Hemisphere and at ∼−73.5° MLAT starting at 14:35 UT in the Southern Hemisphere. The interhemispheric time difference in the TCV signatures are discussed in section 4.

The azimuthal propagation velocity of the transient event is estimated from the magnetic field variations observed by THEMIS-A and THEMIS-E (Figure 6b), both of which were located near the boundary of the magnetopause at a similar radial distance of ∼11 R_E. At the onset of Event 2 (14:30 UT), THEMIS-A was at (10.91, −1.39, 3.20) R_E and THEMIS-E at (11.14, 0.27, 2.70) R_E in the GSE coordinate system. The azimuthal separation between the two spacecraft was 8.8°, which corresponds to ∼10,800 km at the approximate radial location of the two spacecraft (11 R_E, $L = 11.4$, ILAT = 72.8°). The transient event at THEMIS-E led that at THEMIS-A by 40 s, indicating that the propagation is westward (dawnward) at a speed of 270 km/s near the magnetopause. With the same assumption made for the case in Event 1, the equivalent ionospheric propagation velocity near the TCV center is 6.8 km/s on the ground because the longitudinal separation at the ground points is ∼270 km and the time lag is 40 s. GOES-13 and 15 also observed the transient event identified as sudden increases in the B_P component at ∼14:35:00 UT and ∼14:42:30 UT, respectively. The longitudinal separation between the two GOES satellites was ∼60° at the onset of the event, which is equivalent to 44,000 km. Thus, the propagation speed is 98 km/s at 6.6 R_E.

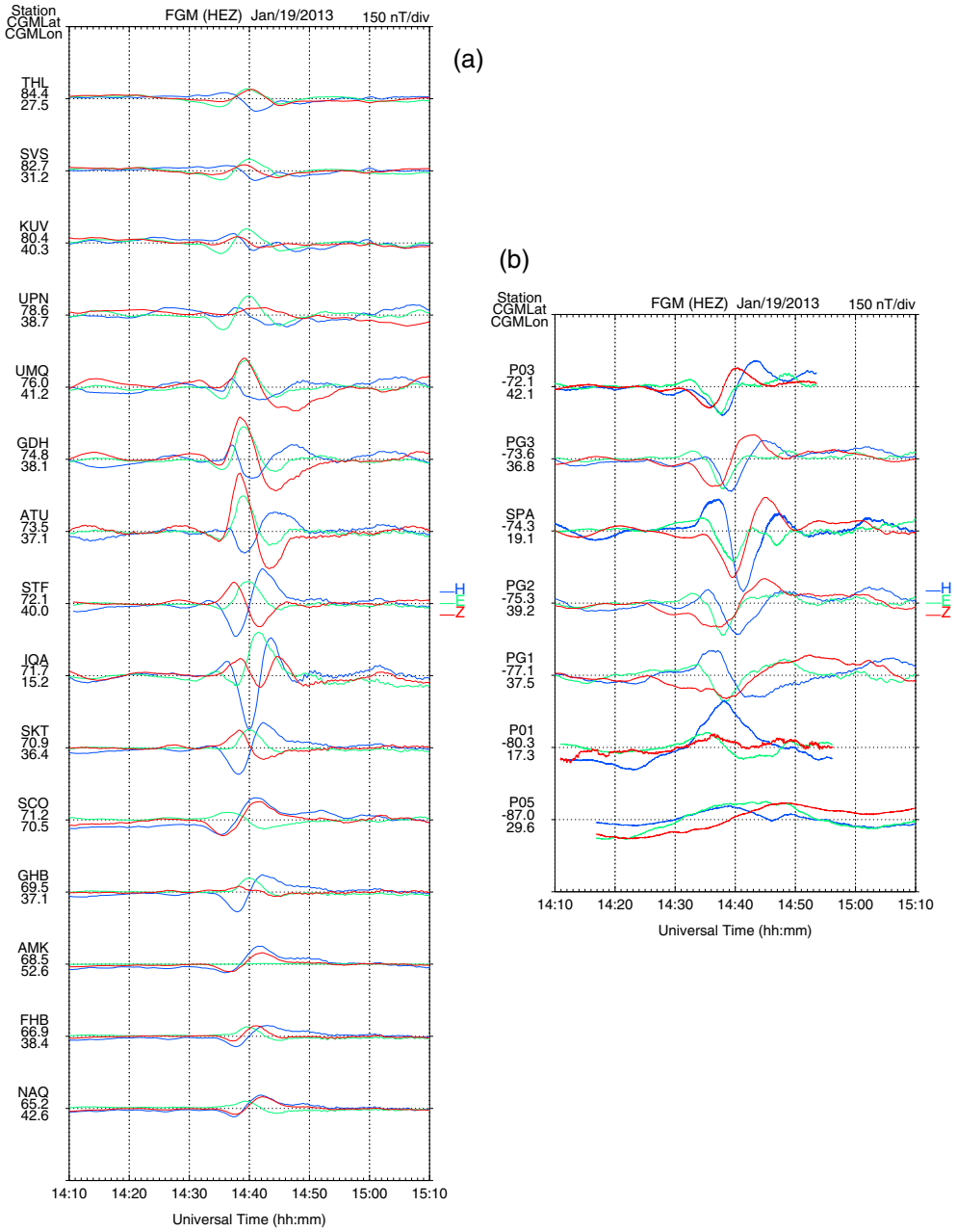

Figure 7. Same as Figure 4 but for Event 2.

As similarly found in Event 1, the longitudinally spaced stations (IQA-STF, SKT-SCO, and SPA-PG3) observed an azimuthal propagation of the event. The propagation is westward (STF to IQA, SCO to SKT, and PG3 to SPA), consistent with the THEMIS observations. The time lags between the stations in the Northern Hemisphere are similar, 131 s between STF and IQA and 141 s between SCO and SKT, yielding 7.0 km/s and 9.8 km/s, respectively (8.4 $\pm$ 1.4 km/s in average). In the Southern Hemisphere, the magnetic signatures at PG3 led that at SPA by 140 s, resulting in a propagation speed of 4.1 km/s, which is lower than those measured in the Northern Hemisphere.

The grey arrows in Figure 8 indicate the approximate durations of the TCV events in each hemisphere. Again, two vortices are observed in the Northern Hemisphere, while only one stretched vortex is seen in the Southern Hemisphere. The duration of the first vortex in the Northern Hemisphere is estimated to be ~300 s, while the vortex in the Southern Hemisphere is ~600 s. Using the average propagation speed in the

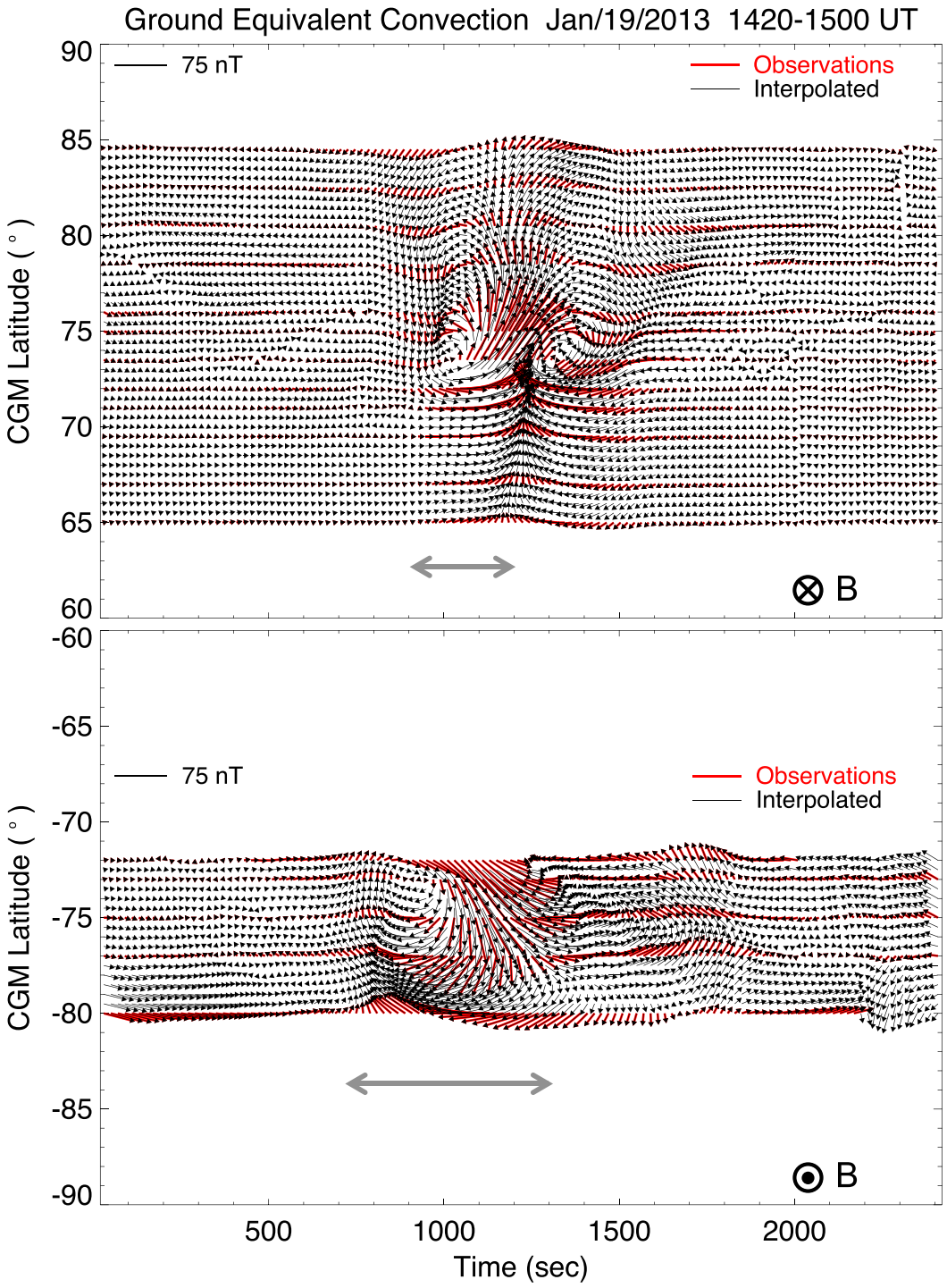

Figure 8. Same as Figure 5 but for Event 2.

Northern Hemisphere (8.4 km/s), the longitudinal size of the vortex is estimated to be ~2500 km. The southern counterpart is also ~2500 km using the propagation speed of 4.1 km/s.%

3.3. Event 3

The third solar wind sudden impulse event at 17:30 UT is shown in the OMNI data, in which an increase in solar wind flow pressure of 4.5 nPa over 5 min is observed (grey box 3 in Figure 6a). The compression of the magnetosphere is also seen from the *SYM-H* index (18 nT over 8 min) as shown in the fifth panel of Figure 6a.

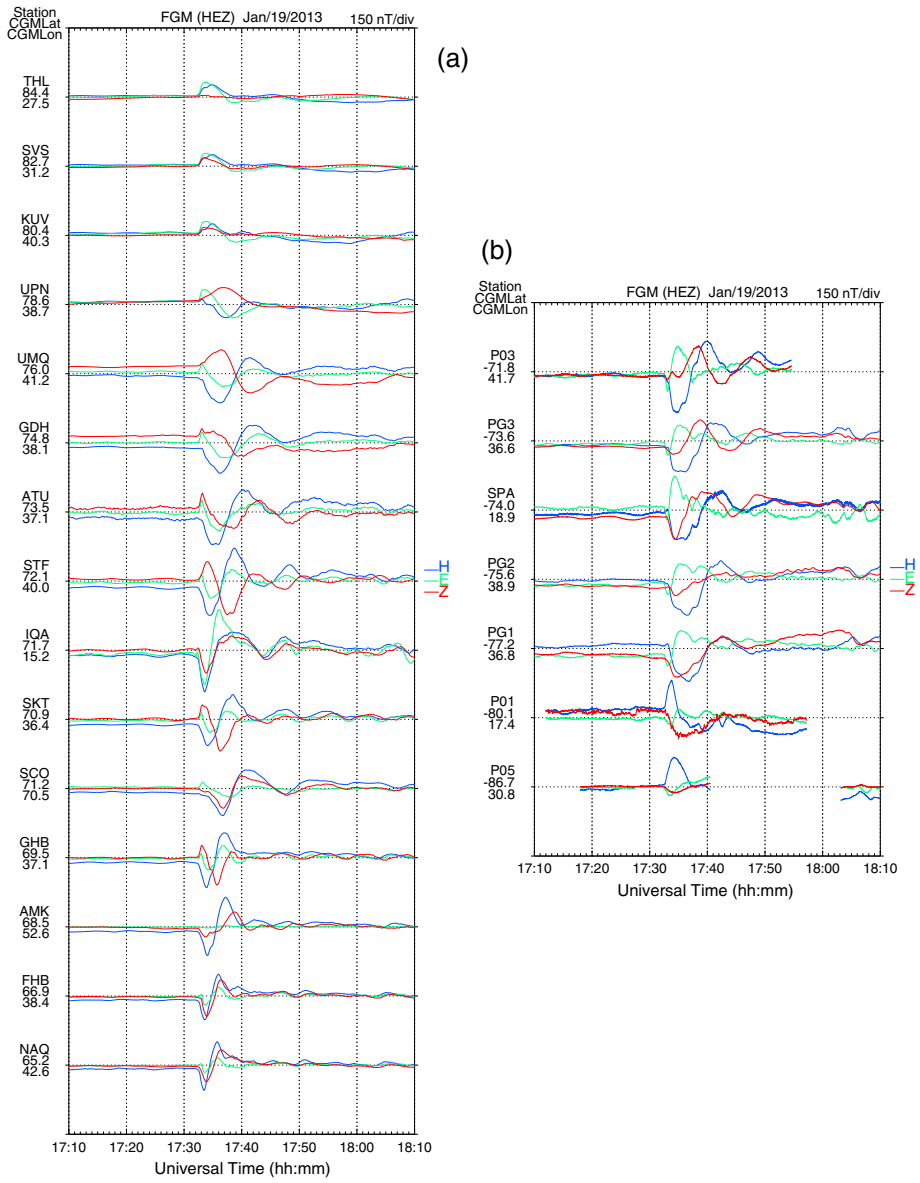

Figure 9. Same as Figure 4 but for Event 3.

There is no remarkable IMF discontinuity except that the IMF B_z increases from 2 nT to 4 nT. Note that $Kp = 2$ during this event.

Like in the previous events shown earlier, the THEMIS spacecraft observed radial motion of the magnetopause in association with the solar wind pressure impulse event at 17:30 UT (Figure 6e). Before the onset of the event, the three spacecraft were located in the magnetosheath (THEMIS-A), near the magnetopause (THEMIS-E), and in the magnetosphere (THEMIS-D) as shown in Figure 6f. At the onset of the event (17:30 UT, grey box 3 in Figure 6e), THEMIS-A entered the solar wind characterized by its weak magnetic field at 12:00 MLT and THEMIS-E the magnetosheath at 12:30 MLT. THEMIS-D, which appears to be far away from the region of the fluctuating magnetic fields, simply observed an increase in the B_z component (30 nT) inside the magnetosphere.

Figure 6d shows magnetic field data from GOES-13 and 15 indicating the compression of the magnetosphere at 17:30 UT during Event 3 (grey box 3). This time, GOES-13 was located near the Sun-Earth line where the radial motion of the magnetopause occurred, and thus the spacecraft observed very well-defined compression. The locations of each spacecraft during Event 3 are displayed in Figure 6f. For the

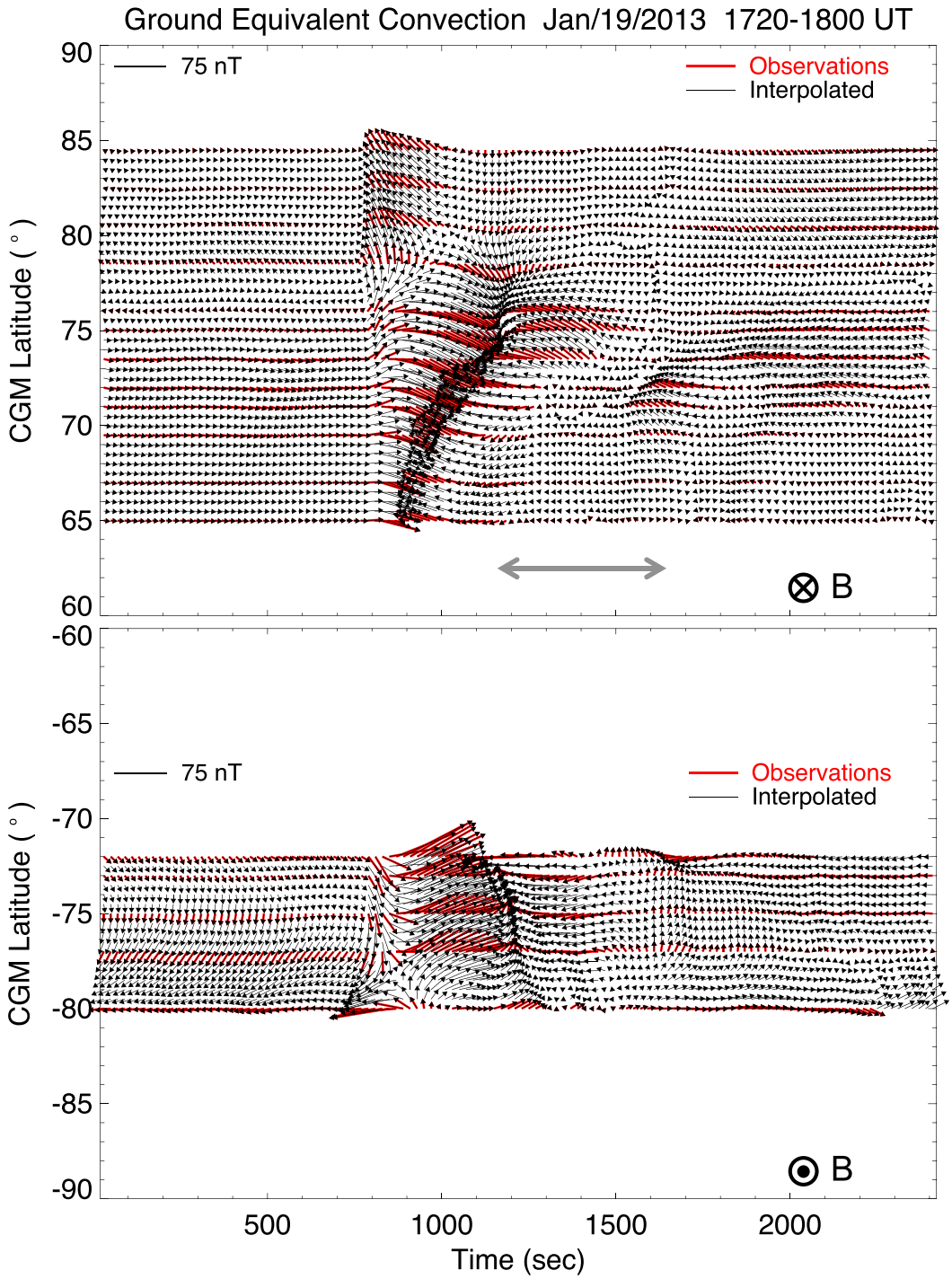

Figure 10. Same as Figure 5 but for Event 3.

magnetopause location during this event, v_{sw} of 420 km/s, n_p of 10.0 cm^{-3}, and B_z of 2 nT are used as the input parameters for the magnetopause model.

Geomagnetic field signatures in response to the solar wind pressure event begin at 17:32 UT (15:32 MLT at 40° magnetic longitude) as shown in Figure 9. Like Event 2, a bipolar structure is clearly seen in the ground data in both hemispheres. It appears that the maximum disturbance is observed near STF at 72.1° MLAT (among the 40° meridional stations) in the Northern Hemisphere and near the region between SPA at −74.3° MLAT and PG3 at −75.6° MLAT in the Southern Hemisphere. The equatorial intersection of the magnetic field of the ground response is marked with the red rectangle in Figure 6f.

Table 2. Summary of the Observations in This Study[a]

	Event 1	Event 2	Event 3
d*Pd*/d*t* (nPa/min) (% change)	0.93 (2800)	0.3 (500)	0.9 (300)
Δ*SYM-H* (nT) (d*SYM-H*/d*t* (nT/min))	40 (2.67)	8 (0.4)	18 (2.25)
Kp	3	1	2
Local time (THEMIS observations)	11:00	11:30	12:30
Local time (Ground observations)	10:30	12:30	15:30
TCV structure (NH; SH[b])	single;single	twin; single	single; none
Transient location observed by THEMIS (deg ILAT)	72.8	72.8	72.4
TCV center location on the ground (MLAT) (NH; SH)	74.0; -76.0	73.5; -73.5	72.0; N/A
TCV propagation direction (ground)	duskward	dawnward	duskward[c]
Propagation velocity measured by THEMIS (km/s)	710	270	92
Equivalent ionospheric propagation velocity inferred from THEMIS (km/s)	17.0	6.8	2.3
TCV propagation velocity (km/s) (NH; SH)	18.4±4.7; 16	8.4±1.4; 4.1	13.2±3.9; ?
Longitudinal extent of TCV (km) (NH; SH)	7700; ?	2500; 2500	6600; N/A

[a]Solar wind dynamic pressure (Pd) is measured by ACE.
[b]NH: Northern Hemisphere; SH: Southern Hemisphere.
[c]THEMIS data show that the propagation is dawnward.

Ionospheric convection flow patterns in association with the solar wind pressure impulse at 17:30 UT during Event 3 are presented in Figure 10. The TCV structure appears to be significantly distorted showing the longitudinally stretched single vortex in the Northern Hemisphere. Though not clearly seen, its center is located at ~72° MLAT between 17:39 and 17:47 UT (see the grey arrow in Figure 10). No noticeable structure is found in the Southern Hemisphere.

At the onset of Event 3 (17:30 UT), THEMIS-A was at (11.36, 0.10, 2.71) R_E and THEMIS-E at (9.86, 1.77, 1.92) R_E in the GSE coordinate system. Unlike the previous two events, the two satellites were not located at a similar R_E near the magnetopause. Therefore, the azimuthal separation is estimated with a very crude assumption that the satellites were at 10.6 R_E (ILAT = 72.4°), the midpoint of the two spacecraft. The separation was 9.7°, which corresponds to ~11,000 km at the approximate radial location of the two spacecraft. The transient event at THEMIS-E led that at THEMIS-A by 120 s, indicating that the propagation is westward (dawnward) at a speed of ~92 km/s near the magnetopause. With the same assumption made for the previous cases, the equivalent ionospheric propagation velocity near the TCV center is 2.3 km/s on the ground because the longitudinal separation at the ground point is ~280 km and the time lag is 120 s. It is also shown that from the GOES-13 and 15 data, the transient event is identified as sudden increases in the B_P component at ~17:32:10 UT and ~17:32:30 UT, respectively. The longitudinal separation between the two GOES satellites was ~62° at the onset of the event, which is equivalent to 46,000 km. The time lag between the events seen by the GOES satellites is only 20 s, yielding a propagation speed much larger than any possible ones in the magnetosphere. This is discussed in section 4.

The ground events from the longitudinally spaced stations observed the azimuthal propagation of the event. In this event, however, the propagation seen on the ground is opposite to that seen in space: IQA to STF, SKT to SCO, and SPA to PG3 (eastward). It should be noted that the local times of the two sets of observations are 3 h apart (THEMIS observations at 12:30 MLT versus ground observations at 15:30 MLT). Therefore, it is possible that the impulse event initiated between the local times propagated away from a common source. This is discussed further in section 4. Similar to the case in Event 1, the propagation speed between the two station pairs in the Northern Hemisphere is significantly different. The time lag between the magnetic disturbances at IQA and STF is 55 s, yielding 17.0 km/s. The data from the second pair in the Northern Hemisphere, SKT and SCO, show that the time lag is 150 s and thus the propagation speed is 9.3 km/s. Thus, the average propagation velocity in the Northern Hemisphere is 13.2 ± 3.9 km/s. In the

Southern Hemisphere, however, the magnetic signatures at SPA led that at PG3 by 4 s, too short to yield any reasonable propagation speed in the ionosphere. It should be noted that the cross correlation between the magnetic signatures at the stations is very high (0.99). This is discussed in section 4.

The grey arrow in Figure 10 indicates the approximate duration (500 s) of the TCV event in the Northern Hemisphere. Using the propagation speed of 9.3 km/s between SKT and SCO, the longitudinal size of the vortex is estimated to be ~4600 km. If the higher propagation speed (17 km/s) obtained from the other pair (IQA-STF) is used, the size is 8500 km. With the limited observations, there is no clear explanation as to why the two propagation speeds are very different and thus there is no justification as to which number should be used for the calculation of the vortex size. Table 2 shows the average size (~6600 km) using the average propagation velocity of 13.2 km/s.

4. Discussion

The events presented here occurred in association with sudden increases in solar wind dynamic pressure. The radial fluctuations of the magnetopause have also been clearly observed by the THEMIS spacecraft near the boundary. A number of studies suggested a close link between MIE/TCV generation and solar wind pressure changes [e.g., *Sibeck et al.*, 1989; *Kivelson and Southwood*, 1991; *Glassmeier and Heppner*, 1992; *Sibeck et al.*, 2003]. It should be noted, of course, that a hot flow anomaly (HFA) at the bow shock associated with a discontinuity in IMF orientation could also be a driver of TCVs as discussed in previous studies [e.g., *Sitar et al.*, 1998; *Kataoka et al.*, 2002; *Jacobsen et al.*, 2009; *Fillingim et al.*, 2011]. *Zesta et al.* [1999] and *Sibeck and Korotova* [1996] suggested that pressure pulses are not an intrinsic feature of the upstream solar wind but are instead created just upstream of the bow shock by a change in IMF orientation, whereas *Sitar et al.* [1996] found no dependence on IMF orientation. In our study, Event 1 showed no noticeable IMF discontinuity, while Events 2 and 3 are associated with IMF discontinuities. We focus primarily on ground signatures in conjugate hemispheres in conjunction with magnetopause deformation and hence did not carry out further investigations as to whether the signatures in the THEMIS data are HFAs. For all the events presented here, it is certain that sudden changes in solar wind dynamic pressure are observed in the pristine solar wind as seen by ACE and OMNI data.

The three events presented in this study are compared interestingly because each event is associated with distinctively different pressure changes in solar wind flow pressure at different local times as summarized in Table 2. The most clearly shaped twin-vortex event (Event 2) occurred with the slowest change in solar wind pressure (0.3 nPa/min) and the modest compression of the magnetosphere (8 nT increase). Although the rate of pressure change of Event 3 is relatively large (0.9 nPa/min), the percent change is relatively small, which is perhaps the reason for creating unapparent vortical structures (the stretched vortex in the Northern Hemisphere and no structure in the Southern Hemisphere). Event 1, showing a single TCV is shown in both hemispheres, is associated with the most extreme solar wind pressure event (0.93 nPa/min, 2800% increase) and largest magnetospheric compression (40 nT increase) among the three events. In addition, all the events in this study occurred during quiet times ($Kp \leq 3$). Previous studies [e.g., *Glassmeier*, 1992; *Lühr et al.*, 1996; *Moretto et al.*, 2002] showed that TCVs have been observed for low *Kp* values, while *Zesta et al.* [2002] found that a significant number of events also occurred during moderate and disturbed times ($3 \leq Kp \leq 6$). Probably, TCV events can be found more easily during quiet times [e.g., *Zesta et al.*, 2002]. Statistical studies have shown that TCVs favor the prenoon ionosphere [e.g., *Glassmeier et al.*, 1989; *Lanzerotti et al.*, 1991; *Zesta et al.*, 2002], which suggests that the local time occurrence of TCVs is controlled by IMF orientation associated with the Parker spiral. The events presented in our study occurred at three distinctively different local times on the ground—Event 1 at 10:30 MLT, Event 2 at 12:30 MLT, and Event 3 at 15:30 MLT. It is not clear, however, whether there is a relationship between the features in TCV structures and local times.

As shown in Table 2, the THEMIS satellites were situated at approximately 72° ILAT during the transient events in this study. The locations of the TCV centers appear to vary, ranging between 72° and 76° MLAT. The latitudinal locations of the TCV centers are in good agreement with the previous studies listed in section 1. The interhemispheric difference in the TCV center locations during Event 1 is 2°, while the TCVs are observed at the same latitude during Event 2. The center location in the south for Event 3 is not seen because no TCV was measured. There is a common feature—the locations of the TCV centers are higher in latitude than those of the transient events seen in space (see the magnetic field intersections of the ground responses in Figures 2d, 6c, and 6f). One of the possible explanations is that the THEMIS spacecraft were not situated where the current systems responsible for the TCV structures were created as they might be located beyond the THEMIS orbit, perhaps in the outer edge of the magnetopause. Additionally, for all the events presented here, the ground responses (shown as initial variations of magnetic field signatures) are observed 2 to

3 min after the transient events seen from the OMNI or THEMIS data. This is interpreted as a field-aligned propagation at an Alfvén speed. It has been observed that magnetospheric compression due to solar wind pressure pulses leads to a global response in the magnetosphere and ionosphere [e.g., *Korotova et al.*, 2002], and the response is quite immediate (for example, ~4 min as reported by *Boudouridis et al.* [2007]).

Previous studies using THEMIS spacecraft also showed similar azimuthal propagation associated with transient events near the magnetopause: for example, 355 km/s [*Jacobsen et al.*, 2009] and 220 km/s [*Korotova et al.*, 2011]. The propagation velocities on the ground are also in agreement with the observations in previous studies: for example, 3–5 km/s [*Friis-Christensen et al.*, 1988], 5.5 km/s [*Glassmeier and Heppner*, 1992], 9.7 km/s [*Sitar et al.*, 1998], and 3–11 km/s [*Zesta et al.*, 2002]. However, it is not clear why the propagation velocities observed between hemispheres are not consistent (see Table 2). Moreover, during Events 1 and 3, the observed propagation velocities are very different even between the two longitudinally spaced stations (IQA-STF and SKT-SCO). Although it is reported that velocities change during propagation [e.g., *Zesta et al.*, 1999], the observations for Events 1 and 3 appear to be too large to be the case. In the study by *Zesta et al.* [2002], TCV events with propagation velocities of >20 km/s were not included in their statistical study because such large velocities when projected into the magnetosphere are much larger than any possible magnetosheath velocity and the velocities correspond to the limit of the timing accuracy between stations based on the method they used. Here we suggest that the discrepancy might be due to an error in correlation analysis performed between the signals from the two stations especially when the signals are disturbed. Another explanation is that the size of the indentation of the magnetopause is similar to or bigger than the distance between the two THEMIS spacecraft (and equivalently the two ground stations), and thus the arrival time difference of the transient events is small, causing the resulting propagation velocity to appear to be unrealistically large.

It has been reported that the longitudinal-scale size of TCV events approximately is in the range of 1500–2500 km [e.g., *Glassmeier et al.*, 1989; *Glassmeier and Heppner*, 1992; *Zesta et al.*, 1999; *Amm et al.*, 2002; *Murr et al.*, 2002]. A statistical study by *Zesta et al.* [2002] also found that the typical scale size of TCV events is of the order of a few thousands of kilometers (approximately between 2000 and 7000 km). It is not clear, however, what controls the size of the structure. Perhaps, the intensity of FACs, that is, the amount of magnetopause deformations associated with pressure increases, might be one of the controlling factors. Event 2, which shows the smallest TCV sizes, is associated with the smallest pressure increase (0.3 nPa/min) and thus smallest compression (8 nT) compared to the other events. Distorted and tilted vortical structures are also observed as shown in the convection patterns and might be attributed to a local enhancement of conductivity due to particle precipitation [e.g., *Friis-Christensen et al.*, 1988], different propagation velocities between the northern and southern parts of the structure [e.g., *Moretto et al.*, 1997; *Zesta et al.*, 1999], and/or different mapping of FAC structures [e.g., *Zesta et al.*, 1999; *Murr et al.*, 2002].

One of the interesting features of the events presented in this paper is well-defined TCV structures observed in the conjugate hemispheres. Observational studies [e.g., *Lanzerotti et al.*, 1990, 1991; *Kataoka et al.*, 2001; *Murr et al.*, 2002; *Kim et al.*, 2013] showed observations of interhemispheric conjugate behavior of MIEs (and TCVs) at high latitudes, suggesting their association with FACs directed in the same direction in both hemispheres. There are many cases in which interhemispheric conjugacy is not well observed partly due to magnetic field mapping between hemispheres [e.g., *Siscoe et al.*, 2001; *Kim et al.*, 2013]. Difference in ionospheric conductivity can also play a role in creating asymmetry in TCV structures [e.g., *Le et al.*, 1993; *Kikuchi et al.*, 2001], which might explain the TCV features shown in our study. A model study by *Zhu et al.* [1997] showed that localized conductivity enhancement due to precipitation associated with the upward FACs can cause a significant distortion of the TCV current system and thus the ground magnetic disturbance patterns. A subsequent study by *Zhu et al.* [1999] suggested that the most favorable condition for strong asymmetry in the TCV ground magnetic signatures is that of winter, solar minimum, and hard precipitation (about 7.8 keV). In fact, it is observed that the southern TCVs in our study are not as well defined as the northern counterpart, although the observation points in the Southern Hemisphere are fewer and there are no further quantitative measures. Our events occurred in January when the solar elevation angles are significantly different between the two conjugate locations. Near ATU and PG3, the conjugate pair where the TCV centers are located, the angles are approximately 20° and 0°, respectively.

The interhemispheric time differences (1 to 2 min) in the TCV signatures during Event 1 (Figure 5) and Event 2 (Figure 8) are another intriguing conjugate feature. *Murr et al.* [2002] also reported a TCV event showing a

time delay between the two hemispheres (IQA-SPA pair) with the event at SPA being delayed by 2 min, while the overall features were similar in shape and amplitude. They explained that the delay might be due to the difference in the length of the field line (using the Tsyganenko model) from the magnetospheric driver to each conjugate location (IQA and SPA) considering Alfvén waves propagating to both hemispheres along the field lines. In fact, their observations were made in July while ours in January, and thus their argument appears reasonable. In our study, however, such a tendency is not found. In Event 1, the TCV signature in the Northern Hemisphere leads the one in the Southern Hemisphere (about 1 min); in Event 2, the southern observation leads the northern counterpart (about 2 min). Again, both events occurred in January. Moreover, a statistical study of MIEs carried out by *Kim et al.* [2013] revealed no clear seasonal dependence on arrival time difference in MIE events. Therefore, a further investigation involving larger data sets is necessary to examine seasonal dependence on asymmetry in TCV features.

As briefly stated in section 1, KHI is also considered as a possible mechanism responsible for generation of TCVs. In fact, one can argue that there are features commonly found in both KHI and transient events: similar latitudinal extent of ground signatures and creation of FACs and their ionospheric responses [e.g., *Dougal et al.*, 2013], and asymmetry in local time occurrences [e.g., *Nykyri*, 2013]. In this paper, however, we stress that solar wind pressure pulse events are the major source of a deformation of the magnetopause which moves along the magnetopause and generates FACs within the magnetosphere—perhaps at the inner edge of the LLBL. These FACs produce TCVs observed in the ionosphere. The following is a summary of our observations supporting the idea: (1) solar wind velocities were not necessarily high for all events; (2) the THEMIS spacecraft observed transient compression near the subsolar magnetopause; and (3) ground data show typical impulsive events (MIEs) and the convection patterns are also transient, not quasi-continuous, which is most likely to be due to transient pressure variations. This seems reinforced by Event 1 which is observed on the morning side (11:00 MLT by THEMIS;10:30 MLT on the ground) with motion toward noon. In addition, during Event 3, THEMIS observed dawnward propagation of the transient compression near noon, while duskward propagation was observed on the ground at 15:30 MLT. This indicates a localized impact point of a transient compression, contrary to the KHI case where propagation is always antisunward.

5. Conclusions

We investigated three transient events associated with solar wind dynamic pressure impulses near the magnetopause and their responses in conjugate hemispheres. The transient events showing radial fluctuations of the magnetopause were observed by the THEMIS spacecraft. Magnetospheric compression during the events was seen by the GOES spacecraft. Geomagnetic signatures seen as TCVs in response to the transient events were observed by the ground magnetometer array in Greenland and Canada and their conjugate locations in Antarctica including recently developed Antarctic magnetometers, mostly located along the 40° magnetic meridian. This new conjugate network provides a unique opportunity to observe geomagnetic field signatures over a relatively large region in both hemispheres. Geomagnetic signatures associated with the transient events during the initial operation of the new ground network are presented in this paper to examine conjugate behavior of ionospheric convection in response to transient events in the magnetosphere.

The ACE (and OMNI) and THEMIS data indicate that the radial fluctuations of the magnetopause were associated with sudden increases in solar wind dynamic pressure (~0.3–0.9 nPa/min). Both *SYM-H* index and GOES magnetic field data show the compression of the magnetosphere. The pressure increase and compression appear to be directly related. This paper features well-defined TCV events in response to the transient events, which were measured simultaneously in the conjugate hemispheres, each of them occurring in the prenoon, noon, and postnoon sectors, respectively. All the events were observed during quiet times ($Kp \leq 3$). The TCV events are characterized by their single or twin vortex, of which the centers are located approximately at 72°–76° MLAT, propagating either dawnward or duskward. While interhemispheric conjugacy is expected with an assumption that TCV signatures are created by FACs directed in both hemispheres, our observations suggest that there might be more complex mechanisms contributing the asymmetrical features, perhaps due to field line mapping and/or conductivity differences. A statistical approach might be necessary to understand conjugate behavior of TCV events.

Acknowledgments
Support for this research has been provided by the National Science Foundation through grants to Virginia Tech: ATM-0922979 for the development of the Antarctic measurement systems that provided the data and NSF grants ANT-0839588 and PLR-1243398 that have supported the continuing operation of the measurement program, acquisition and processing of the data, and scientific analysis of the data. The work of M. J. Engebretson was supported by NSF grant, PLR-1341493 to Augsburg College. The OMNI and THEMIS data were obtained and processed using THEMIS Data Analysis Software (TDAS). We acknowledge NASA contract NAS5-02099 and V. Angelopoulos for use of data from the THEMIS Mission. Specifically, we thank K. H. Glassmeier, U. Auster, and W. Baumjohann for the use of FGM data provided under the lead of the Technical University of Braunschweig and with financial support through the German Ministry for Economy and Technology and the German Center for Aviation and Space (DLR) under contract 50 OC 0302. The ACE and Cluster data were provided from Coordinated Data Analysis Web (CDAWeb) at http://cdaweb.gsfc.nasa.gov. The GOES data were accessed using the data archive at NOAA Space Weather Prediction Center (http://www.swpc.noaa.gov). The magnetic field tracing tool (IDL GEOPACK DLM) is provided by Haje Korth at Applied Physics Laboratory, Johns Hopkins University. We would like to thank the following persons/institutes for providing ground magnetometer data: Jeff Love at USGS Geomagnetism Program and Lorne McKee at Natural Resources Canada for the INTERMAGNET data (IQA), DTU Space for the Greenland magnetometer data, GFZ Potsdam and Observatory Niemegk for the *Kp* index, and Polar Experiment Network for Geospace Upper-atmosphere Investigations (PENGUIn) team for the AGO and South Pole data.

Michael Balikhin thanks the reviewers for their assistance in evaluating this paper.

References

Amm, O., M. J. Engebretson, T. Hughes, L. Newitt, A. Viljanen, and J. Watermann (2002), A traveling convection vortex event study: Instantaneous ionospheric equivalent currents, estimation of field-aligned currents, and the role of induced currents, *J. Geophys. Res.*, *107*(A11), 1334, doi:10.1029/2002JA009472.

Araki, T. (1977), Global structure of geomagnetic sudden commencements, *Planet. Space Sci.*, *25*, 373–384, doi:10.1016/0032-0633(77)90053-8.

Auster, H. U., et al. (2008), The THEMIS fluxgate magnetometer, *Space Sci. Rev.*, *141*, 235–264, doi:10.1007/s11214-008-9365-9.

Balogh, A., et al. (1997), The Cluster magnetic field investigation, *Space Sci. Rev.*, *79*, 65–91, doi:10.1023/A:1004970907748.

Boudouridis, A., L. R. Lyons, E. Zesta, and J. M. Ruohoniemi (2007), Dayside reconnection enhancement resulting from a solar wind dynamic pressure increase, *J. Geophys. Res.*, *112*, A06201, doi:10.1029/2006JA012141.

Clauer, C. R. (2003), Ionospheric observations of waves at the inner edge of the low latitude boundary layer, in *Earth's Low-Latitude Boundary Layer, Geophys. Monogr, Ser.*, vol. 133, edited by P. T. Newell and T. Onsager, pp. 297–309, AGU, Washington, D. C., doi:10.1029/133GM30.

Clauer, C. R., and V. G. Petrov (2002), A statistical investigation of traveling convection vortices observed by the west coast Greenland magnetometer chain, *J. Geophys. Res.*, *107*(A7), 1148, doi:10.1029/2001JA000228.

Clauer, C. R., and A. J. Ridley (1995), Ionospheric observations of magnetospheric low-latitude boundary layer waves on August 4, 1991, *J. Geophys. Res.*, *100*, 21,873–21,884, doi:10.1029/95JA00678.

Clauer, C. R., et al. (2014), An autonomous adaptive low-power instrument platform (AAL-PIP) for remote high-latitude geospace data collection, *Geosci. Instrum. Methods Data Syst.*, *3*, 211–227, doi:10.5194/gi-3-211-2014.

Cowley, S. W. H. (2000), Magnetosphere-ionosphere interactions: A tutorial review, in *Magnetospheric Current Systems*, vol. 118, edited by S.-I. Ohtani et al., 91 pp., AGU, Washington, D. C.

Dougal, E. R., K. Nykyri, and T. W. Moore (2013), Mapping of the quasi-periodic oscillations at the flank magnetopause into the ionosphere, *Ann. Geophys.*, *31*, 1993–2011, doi:10.5194/angeo-31-1993-2013.

Engebretson, M. J., et al. (2013), Multi-instrument observations from Svalbard of a traveling convection vortex, electromagnetic ion cyclotron wave burst, and proton precipitation associated with a bow shock instability, *J. Geophys. Res. Space Physics*, *118*, 2975–2997, doi:10.1002/jgra.50291.

Fairfield, D. H. (1971), Average and unusual locations of the Earth's magnetopause and bow shock, *J. Geophys. Res.*, *76*, 6700–6716, doi:10.1029/JA076i028p06700.

Fillingim, M. O., J. P. Eastwood, G. K. Parks, V. Angelopoulos, I. R. Mann, S. B. Mende, and A. T. Weatherwax (2011), Polar UVI and THEMIS GMAG observations of the ionospheric response to a hot flow anomaly, *J. Atmos. Sol. Terr. Phys.*, *73*, 137–145, doi:10.1016/j.jastp.2010.03.001.

Friis-Christensen, E., S. Vennerstrom, M. A. McHenry, and C. R. Clauer (1988), Ionospheric traveling convection vortices observed near the polar cleft—A triggered response to sudden changes in the solar wind, *Geophys. Res. Lett.*, *15*, 253–256, doi:10.1029/GL015i003p00253.

Fukushima, N. (1969), Equivalence in ground geomagnetic effect of Chapman-Vestine's and Birkeland-Alfvén's current systems for polar magnetic storms, *Rep. Ionos. Space Res. Jap.*, *23*, 219–227.

Glassmeier, K.-H. (1992), Traveling magnetospheric convection twin-vortices—Observations and theory, *Ann. Geophys.*, *10*, 547–565.

Glassmeier, K.-H., and C. Heppner (1992), Traveling magnetospheric convection twin vortices—Another case study, global characteristics, and a model, *J. Geophys. Res.*, *97*, 3977–3992, doi:10.1029/91JA02464.

Glassmeier, K.-H., M. Hoenisch, and J. Untiedt (1989), Ground-based and satellite observations of traveling magnetospheric convection twin vortices, *J. Geophys. Res.*, *94*, 2520–2528, doi:10.1029/JA094iA03p02520.

Goertz, C. K., E. Nielsen, A. Korth, C. Haldoupis, P. Hoeg, D. Hayward, and K. H. Glassmeier (1985), Observations of a possible ground signature of flux transfer events, *J. Geophys. Res.*, *90*, 4069–4078, doi:10.1029/JA090iA05p04069.

Jacobsen, K. S., et al. (2009), THEMIS observations of extreme magnetopause motion caused by a hot flow anomaly, *J. Geophys. Res.*, *114*, A08210, doi:10.1029/2008JA013873.

Kataoka, R., H. Fukunishi, L. J. Lanzerotti, C. G. Maclennan, H. U. Frey, S. B. Mende, J. H. Doolittle, T. J. Rosenberg, and A. T. Weatherwax (2001), Magnetic impulse event: A detailed case study of extended ground and space observations, *J. Geophys. Res.*, *106*, 25,873–25,890, doi:10.1029/2000JA000314.

Kataoka, R., H. Fukunishi, L. J. Lanzerotti, T. J. Rosenberg, A. T. Weatherwax, M. J. Engebretson, and J. Watermann (2002), Traveling convection vortices induced by solar wind tangential discontinuities, *J. Geophys. Res.*, *107*(A12), 1455, doi:10.1029/2002JA009459.

Kataoka, R., H. Fukunishi, and L. J. Lanzerotti (2003), Statistical identification of solar wind origins of magnetic impulse events, *J. Geophys. Res.*, *108*(A12), 1436, doi:10.1029/2003JA010202.

Kataoka, R., H. Fukunishi, S. Fujita, T. Tanaka, and M. Itonaga (2004), Transient response of the Earth's magnetosphere to a localized density pulse in the solar wind: Simulation of traveling convection vortices, *J. Geophys. Res.*, *109*, A03204, doi:10.1029/2003JA010287.

Kikuchi, T., S. Tsunomura, K. Hashimotsolar, and K. Nozaki (2001), Field-aligned current effects on midlatitude geomagnetic sudden commencements, *J. Geophys. Res.*, *106*, 15,555–15,566, doi:10.1029/2001JA900030.

Kim, H., X. Cai, C. R. Clauer, B. S. R. Kunduri, J. Matzka, C. Stolle, and D. R. Weimer (2013), Geomagnetic response to solar wind dynamic pressure impulse events at high-latitude conjugate points, *J. Geophys. Res. Space Physics*, *118*, 6055–6071, doi:10.1002/jgra.50555.

King, J. H., and N. E. Papitashvili (2005), Solar wind spatial scales in and comparisons of hourly Wind and ACE plasma and magnetic field data, *J. Geophys. Res.*, *110*, A02104, doi:10.1029/2004JA010649.

Kivelson, M. G., and D. J. Southwood (1991), Ionospheric traveling vortex generation by solar wind buffeting of the magnetosphere, *J. Geophys. Res.*, *96*, 1661–1667, doi:10.1029/90JA01805.

Korotova, G. I., D. G. Sibeck, H. J. Singer, and T. J. Rosenberg (2002), Tracking transient events through geosynchronous orbit and in the high-latitude ionosphere, *J. Geophys. Res.*, *107*(A11), 1345, doi:10.1029/2002JA009477.

Korotova, G. I., D. G. Sibeck, A. Weatherwax, V. Angelopoulos, and V. Styazhkin (2011), THEMIS observations of a transient event at the magnetopause, *J. Geophys. Res.*, *116*, A07224, doi:10.1029/2011JA016606.

Lanzerotti, L. J., A. Wolfe, C. G. Maclennan, L. V. Medford, and R. D. Hunsucker (1987), Ionosphere and ground-based response to field-aligned currents near the magnetospheric cusp regions, *J. Geophys. Res.*, *92*, 7739–7743, doi:10.1029/JA092iA07p07739.

Lanzerotti, L. J., A. Wolfe, N. Trivedi, C. G. Maclennan, and L. V. Medford (1990), Magnetic impulse events at high latitudes—Magnetopause and boundary layer plasma processes, *J. Geophys. Res.*, *95*, 97–107, doi:10.1029/JA095iA01p00097.

Lanzerotti, L. J., C. G. Maclennan, R. M. Konik, A. Wolfe, and D. Venkatesan (1991), Cusp latitude magnetic impulse events. I—Occurrence statistics, *J. Geophys. Res.*, *96*, 14,009–14,022, doi:10.1029/91JA00567.

Le, G., C. T. Russell, S. M. Petrinec, and M. Ginskey (1993), Effect of sudden solar wind dynamic pressure changes at subauroral latitudes—Change in magnetic field, *J. Geophys. Res.*, *98*, 3983–3990, doi:10.1029/92JA02397.
Lee, D.-Y., and L. R. Lyons (2004), Geosynchronous magnetic field response to solar wind dynamic pressure pulse, *J. Geophys. Res.*, *109*, A04201, doi:10.1029/2003JA010076.
Lühr, H., M. Lockwood, P. E. Sandholt, T. L. Hansen, and T. Moretto (1996), Multi-instrument ground-based observations of a travelling convection vortices event, *Ann. Geophys.*, *14*, 162–181, doi:10.1007/s00585-996-0162-z.
McHenry, M. A., and C. R. Clauer (1987), Modeled ground magnetic signatures of flux transfer events, *J. Geophys. Res.*, *92*, 11,231–11,240, doi:10.1029/JA092iA10p11231.
McHenry, M. A., C. R. Clauer, E. Friis-Christensen, P. T. Newell, and J. D. Kelly (1990), Ground observations of magnetospheric boundary layer phenomena, *J. Geophys. Res.*, *95*, 14,995–15,005, doi:10.1029/JA095iA09p14995.
Moretto, T., and A. Yahnin (1998), Mapping travelling convection vortex events with respect to energetic particle boundaries, *Ann. Geophys.*, *16*, 891–899, doi:10.1007/s00585-998-0891-2.
Moretto, T., E. Friis-Christensen, H. Lühr, and E. Zesta (1997), Global perspective of ionospheric traveling convection vortices: Case studies of two Geospace Environmental Modeling events, *J. Geophys. Res.*, *102*, 11,597–11,610, doi:10.1029/97JA00324.
Moretto, T., M. Hesse, A. Yahnin, A. Ieda, D. Murr, and J. F. Watermann (2002), Magnetospheric signature of an ionospheric traveling convection vortex event, *J. Geophys. Res.*, *107*(A6), 1072, doi:10.1029/2001JA000049.
Murr, D. L., and W. J. Hughes (2003), Solar wind drivers of traveling convection vortices, *Geophys. Res. Lett.*, *30*(7), 1354, doi:10.1029/2002GL015498.
Murr, D. L., W. J. Hughes, A. S. Rodger, E. Zesta, H. U. Frey, and A. T. Weatherwax (2002), Conjugate observations of traveling convection vortices: The field-aligned current system, *J. Geophys. Res.*, *107*(A10), 1306, doi:10.1029/2002JA009456.
Musko, S. B., C. R. Clauer, A. J. Ridley, and K. L. Arnett (2009), Autonomous low-power magnetic data collection platform to enable remote high latitude array deployment, *Rev. Sci. Instrum.*, *80*, 044501, doi:10.1063/1.3108527.
Nykyri, K. (2013), Impact of MHD shock physics on magnetosheath asymmetry and Kelvin-Helmholtz instability, *J. Geophys. Res. Space Physics*, *118*, 5068–5081, doi:10.1002/jgra.50499.
Rosenberg, T. J., and J. H. Doolittle (1994), Studying the polar ionosphere and magnetosphere with Automatic Geophysical Observatories: The United States program in Antarctica, *Antarct. J. U. S.*, *29*(5), 347–349.
Russell, C. T., M. Ginskey, and S. M. Petrinec (1994), Sudden impulses at low-latitude stations: Steady state response for northward interplanetary magnetic field, *J. Geophys. Res.*, *99*, 253–261, doi:10.1029/93JA02288.
Shue, J.-H., J. K. Chao, H. C. Fu, C. T. Russell, P. Song, K. K. Khurana, and H. J. Singer (1997), A new functional form to study the solar wind control of the magnetopause size and shape, *J. Geophys. Res.*, *102*, 9497–9512, doi:10.1029/97JA00196.
Sibeck, D. G. (1993), Transient magnetic field signatures at high latitudes, *J. Geophys. Res.*, *98*, 243–256, doi:10.1029/92JA01661.
Sibeck, D. G., and G. I. Korotova (1996), Occurrence patterns for transient magnetic field signatures at high latitudes, *J. Geophys. Res.*, *101*, 13,413–13,428, doi:10.1029/96JA00187.
Sibeck, D. G., R. E. Lopez, and W. Baumjohann (1989), Solar wind dynamic pressure variations and transient magnetospheric signatures, *Geophys. Res. Lett.*, *16*, 13–16, doi:10.1029/GL016i001p00013.
Sibeck, D. G., N. B. Trivedi, E. Zesta, R. B. Decker, H. J. Singer, A. Szabo, H. Tachihara, and J. Watermann (2003), Pressure-pulse interaction with the magnetosphere and ionosphere, *J. Geophys. Res.*, *108*(A2), 1095, doi:10.1029/2002JA009675.
Siscoe, G. L., G. M. Erickson, B. U. Ö. Sonnerup, N. C. Maynard, K. D. Siebert, D. R. Weimer, and W. W. White (2001), Global role of $E_{\|}$ in magnetopause reconnection: An explicit demonstration, *J. Geophys. Res.*, *106*, 13,015–13,022, doi:10.1029/2000JA000062.
Sitar, R. J., C. R. Clauer, and E. Friis-Christensen (1996), High-latitude ground-based response to sudden changes in solar wind dynamic pressure, *J. Geophys. Res.*, *101*, 27,001–27,014, doi:10.1029/96JA02799.
Sitar, R. J., J. B. Baker, C. R. Clauer, A. J. Ridley, J. A. Cumnock, V. O. Papitashvili, J. Spann, M. J. Brittnacher, and G. K. Parks (1998), Multi-instrument analysis of the ionospheric signatures of a hot flow anomaly occurring on July 24, 1996, *J. Geophys. Res.*, *103*, 23,357–23,372, doi:10.1029/98JA01916.
Tsyganenko, N. A. (2002a), A model of the near magnetosphere with a dawn-dusk asymmetry 1. Mathematical structure, *J. Geophys. Res.*, *107*(A8), 1179, doi:10.1029/2001JA000219.
Tsyganenko, N. A. (2002b), A model of the near magnetosphere with a dawn-dusk asymmetry 2. Parameterization and fitting to observations, *J. Geophys. Res.*, *107*(A8), 1176, doi:10.1029/2001JA000220.
Turner, D. L., et al. (2011), Multispacecraft observations of a foreshock-induced magnetopause disturbance exhibiting distinct plasma flows and an intense density compression, *J. Geophys. Res.*, *116*, A04230, doi:10.1029/2010JA015668.
Villante, U., and M. Piersanti (2011), Sudden impulses at geosynchronous orbit and at ground, *J. Atmos. Sol. Terr. Phys.*, *73*, 61–76, doi:10.1016/j.jastp.2010.01.008.
Zesta, E., W. J. Hughes, M. J. Engebretson, T. J. Hughes, A. J. Lazarus, and K. I. Paularena (1999), The November 9, 1993, traveling convection vortex event: A case study, *J. Geophys. Res.*, *104*, 28,041–28,058, doi:10.1029/1999JA900306.
Zesta, E., W. J. Hughes, and M. J. Engebretson (2002), A statistical study of traveling convection vortices using the Magnetometer Array for Cusp and Cleft Studies, *J. Geophys. Res.*, *107*(A10), 1317, doi:10.1029/1999JA000386.
Zhang, H., D. G. Sibeck, Q.-G. Zong, J. P. McFadden, D. Larson, K.-H. Glassmeier, and V. Angelopoulos (2012), Global magnetospheric response to an interplanetary shock: THEMIS observations, *Ann. Geophys.*, *30*, 379–387, doi:10.5194/angeo-30-379-2012.
Zhu, L., P. Gifford, J. J. Sojka, and R. W. Schunk (1997), Model study of ground magnetic signatures of traveling convection vortices, *J. Geophys. Res.*, *102*, 7449–7460, doi:10.1029/96JA03682.
Zhu, L., R. W. Schunk, and J. J. Sojka (1999), Effects of magnetospheric precipitation and ionospheric conductivity on the ground magnetic signatures of traveling convection vortices, *J. Geophys. Res.*, *104*, 6773–6782, doi:10.1029/1998JA900175.